Angular Distribution Measurement and Shower Study in the Soudan Underground Laboratory using an Active Muon Veto Shield

by

Nathaniel J. Pastika

Senior Thesis Project for Bachelors of Science in Physics in the

Department of Physics, Institute of Technology at the

University of Minnesota - Minneapolis

Advisor:

Priscilla Cushman

Spring 2008

Angular Distribution Measurement and Shower Study in the Soudan Underground Laboratory using an Active Muon Veto Shield

Nathaniel J. Pastika

Abstract

Angular Distribution Measurement and Shower Study in the Soudan Underground Laboratory using an Active Muon Veto Shield

by

Nathaniel J. Pastika

Bachelors of Science in Physics

Department of Physics, Institute of Technology

University of Minnesota - Minneapolis

Advisor, Priscilla Cushman

Spring 2008

The Soudan Low Background Counting Facility is a new user oriented installation in the Soudan Underground Laboratory which provides a large experimental area covered with an active muon veto shield. This veto shield, which remains from the proton decay experiment, has been refurbished and a new data acquisition system has been implemented. This shield has been used to measure the angular distribution of muons at the Soudan Laboratory. In the range of the shield we see a 30 ± 6% higher muon flux in the north-south direction than the east-west direction. We also measured the full zenith distribution in the east-west direction.

We have also begun a study of high multiplicity showers in the shield as well in preparation for the instillation of the Neutron Multiplicity Meter. This shower data and the Neutron Multiplicity Meter will be used to study high energy neutrons and the electromagnetic showers that accompany them.

Acknowledgements

I would like to Prisca for giving me a job three years ago and keeping me employed all this time even if I was not sure who was paying me in the beginning. I would also like to thank Prisca for being my advisor on this project and providing the resources to get it done. It is always nice to know there is someone searching for money in the never ending funding was, and even better this person is not me. Who know I could live at home over the summer in the middle of nowhere and work at a full service physics lab.

I would also like to thank Dan Pearson, John Bongaarts, Kyle Johnson and all the other students who helped with the refurbishment of the shield and the ever unforgettable washing of lead bricks. The entire DAQ system would also be nonexistent without Brian Sherwood's design.

I would like to thank the Soudan Mine crew who were all willing to bend over backward to help me and all the other annoying undergrads bothering them for help on this or that. I especially want to thank Jim Beaty without whom would be blundering in the dark. His knowledge of the shield, the lab, and the way to get the job done are second to none. Many an hour of searching for the proper tool or object has been saved by asking Jim what and where to find it.

This project would not be possible without any of these contributors and many others. Thanks everyone, and hopefully you will all continue to provide your indispensable help for a long time to come.

Table of Contents

Chapter 1

Introduction 1

1.1 Soudan Underground Laboratory 2

1.2 Low Background Counting Facility 2

Chapter 2

Soudan LBCF Vetoshield 4

2.1 Vetoshield summary 4

2.2 Gas handling system 7

2.3 Gas control system 9

Chapter 3

Data Acquisition System 10

3.1 DAQ introduction 10

3.2 First generation DAQ 11

3.3 Second generation DAQ 12

3.4 DAQ Timing 14

3.5 DAQ software 16

3.6 Trigger configuration 17

3.7 Veto tube efficiency 19

Chapter 4

Angular distribution measurements 21

4.1 Angular measurements 21

4.2 Experimental setup 21

4.3 Angular distribution decomposition 24

4.4 Angle error analysis 25

4.5 Azimuthal angle data 27

4.6 Zenith expectations 28

4.7 Zenith angle Monte Carlo 29

4.8 Zenith angle data 31

4.9 Angle conclusion 36

Chapter 5

High Multiplicity Measurements 38

5.1 High multiplicity introduction 38

5.2 High multiplicity data 38

5.3 Neutron Multiplicity Meter 43

Chapter 6

Conclusion 45

Bibliography 46

Chapter 1

Introduction

With modern experiments in search of dark matter, double beta-decay, and other high precision, low background experiments, there is no choice but to go underground. Beyond simply placing these experiments underground, the detectors must be constructed of very pure materials which are very difficult to fabricate. Many materials can even be rendered useless by activation from surface level background. These limitations on even the production and storage of such materials give rise to the need for deep underground low background counting facilities. Facilities of this type can provide the ability to test, store, and fabricate materials for low background experiments, as well as serve as areas to test prototype detectors. In order to fulfill the needs for such facilities a low background counting facility has been put in place at the University of Minnesota's Soudan Underground Laboratory.

The Soudan LBCF is located in the former proton decay experiment hall of the Soudan Laboratory. The proton decay calorimeter was removed from the hall leaving a large space that is surrounded with the muon vetoshield installed with the proton decay experiment. This hall contains a large area for various users to place and test/run their detectors as well as a number of general use detectors. The general use facilities include a clean room, general use low background detectors, as well as a full coverage muon vetoshield.

In order to better understand the environment of this new low background counting facility, we have used the muon vetoshield in order to measure the angular distribution of the muons at the Soudan laboratory. These measurements can be used to create more accurate monte carlo simulations by giving a benchmark for these simulations to create their muon distributions with. Furthermore, these angular distributions can be used to understand the overburden of the.

On top of these angular distribution measurements, we have also started a study of high multiplicity hadronic showers with the vetoshield. These showers are of particular interest because of

the high energy neutrons that can accompany these showers. High energy neutrons, above about 60 MeV, are dangerous sources of background for many "zero background" experiments such as CDMS. Researchers working on these projects have tried to quantify these backgrounds with monte carlo simulations, but there are major differences between the leading monte carlo codes of Geant4 and fluka as well as discrepancies with actual measurements [1]. We hope that the events we see in the shield as well as information from a neutron detector to be installed later this year will allow us to unravel this mystery.

1.1 Soudan Underground Laboratory

The Soudan Underground Laboratory is a deep underground physics laboratory located in the old Soudan Iron Mine turned state park. The lab is operated by the University of Minnesota and is located on the 27th level of the mine which is 2341 ft below the surface. The Soudan Laboratory originally hosted the Soudan II experiment and now hosts MINOS, CDMS and Soudan LBCF. The lab layout is shown in figure 1. The overburden above the lab gives an average equivalent depth of 2190 ± 160 m.w.e. [2].

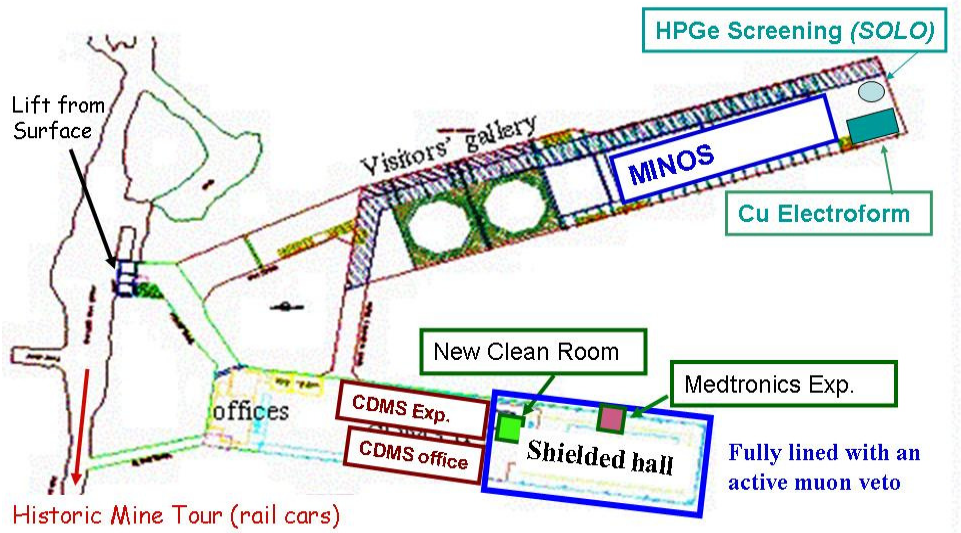

Figure 1. The Soudan Underground Laboratory layout [3].

1.2 Low Background Counting Facility

The Soudan Low Background Counting Facility is located in the Soudan II hall, pictured in figure 2. The old proton decay calorimeter was removed leaving a 13 by 40 by 10 meter hall open for use. This hall is already equipped with power, network and other needed infrastructure, such as a seven ton crane, for lab setup which significantly reduces the cost of such an installation. The entire space will be open for the placement of prototype detector or small scale experiments. A new clean room has been constructed on the raised mezzanine to more sensitive detectors. The LBCF will also feature a number of general use detectors for low background counting including alpha, beta, and gamma screening. The entire hall is lined with an active muon vetoshield which will provide veto triggers and muon path information to users of the facility.

Figure 2. This is a photo of the LBCF hall. The clean room can be seen in the upper right and the veto tubes can be seen lining the walls.

Chapter 2

Soudan LBCF Vetoshield

2.1 Vetoshield summary

The muon vetoshield is the original shield from the proton decay experiment which inhabited the experimental hall prior to the low background counting facility. This shield and the original DAQ system were designed at Tuffs University for use with the Soudan II proton decay calorimeter. The shield consists of more than 1000 proportional tubes which surround the entire room. Each of the tubes is 9.6 by 21.0 cm and is one to seven meters in length depending on the place it was needed to fill. The tubes are constructed with eight hexagonal wire chambers which each contain a single gold wire strung down the center of each wire chamber, shown in figure 3. The tubes have two layers of four wire chambers. There is an offset of the inner and outer channels allowing the tubes to be placed in continuous panels without any gaps in the coverage.

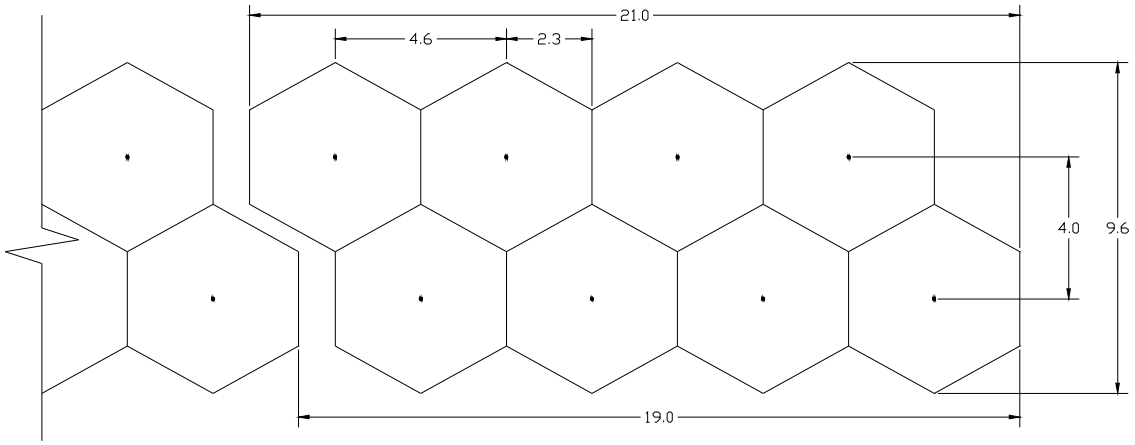

Figure 3. This is a schematic cross-section of a veto tube. The dimensions are given in centimeters.

Each tube is readout by a two channel preamp card which reads the inner four wires as one channel and the outer four wires as the second. This configuration allows for two layers and therefore the ability to take coincidents for every section of the shield. The preamp is supplied with a voltage of about 2400V charges the wires through 30 MΩ. The preamp cards are also provided with a 5V and -7V to power the amplifiers and other circuit elements. The preamp amplifies the signals from the signal wires and then passes them into a fixed threshold comparator/amplifier. From the amplifier the signals are repeated by a one-shot with a length of about 1.2 μs and then converted to a differential signal to be transmitted to the data acquisition system.

The vetoshield covers the entire surface of the ceiling and walls of the hall with the exception of the access doors in the north wall. The majority of the shield is constructed of panels of 7m long tubes which are placed horizontally around the room and along the ceiling. The wall panels, 12 in total, each contain 50 tubes while each of the 2 ceiling panels contains 166 tubes. This layout is demonstrated in figure 4. The ceiling has a small overhang on the walls to provide gap coverage on the wall/ceiling interface. The gaps between adjacent wall panels are covered by vertically hanging tubes which are mounted on sliding brackets so the ends of the tubes behind them can be accessed at need. These sliding panels consist of 6 or 8 tubes. The main entry way in the north wall is shadowed by a large set of tubes set farther inside the hall to provide coverage around the opening. Currently the eighth of the ceiling above the clean room is covered by a second layer of tubes which are set orthogonally to the primary set of tubes on the ceiling. Although all the ceiling is not implemented in this way, there are sufficient number of spare tubes to implement this in other areas of the ceiling if not the entire ceiling.

The high voltage for the tubes is provided by +5KV Bertan supplies designed for use with proportional wire chambers. The Shield is divided into 4 sections. Each section is powered by one high voltage power supply. The high voltage power supplies provide the voltage to a breakout box where it is sent out to each panel individually. Among individual tubes in a panel the high voltage is jumped from one tube to the next. The low voltage is provided by two individual power supplies, one for the +5V and the other for the -7V lines required by the preamps. Like the high voltage supplies the low voltage is split into four sections and is first sent though a breakout box where the lines are then distributed to the individual panels.

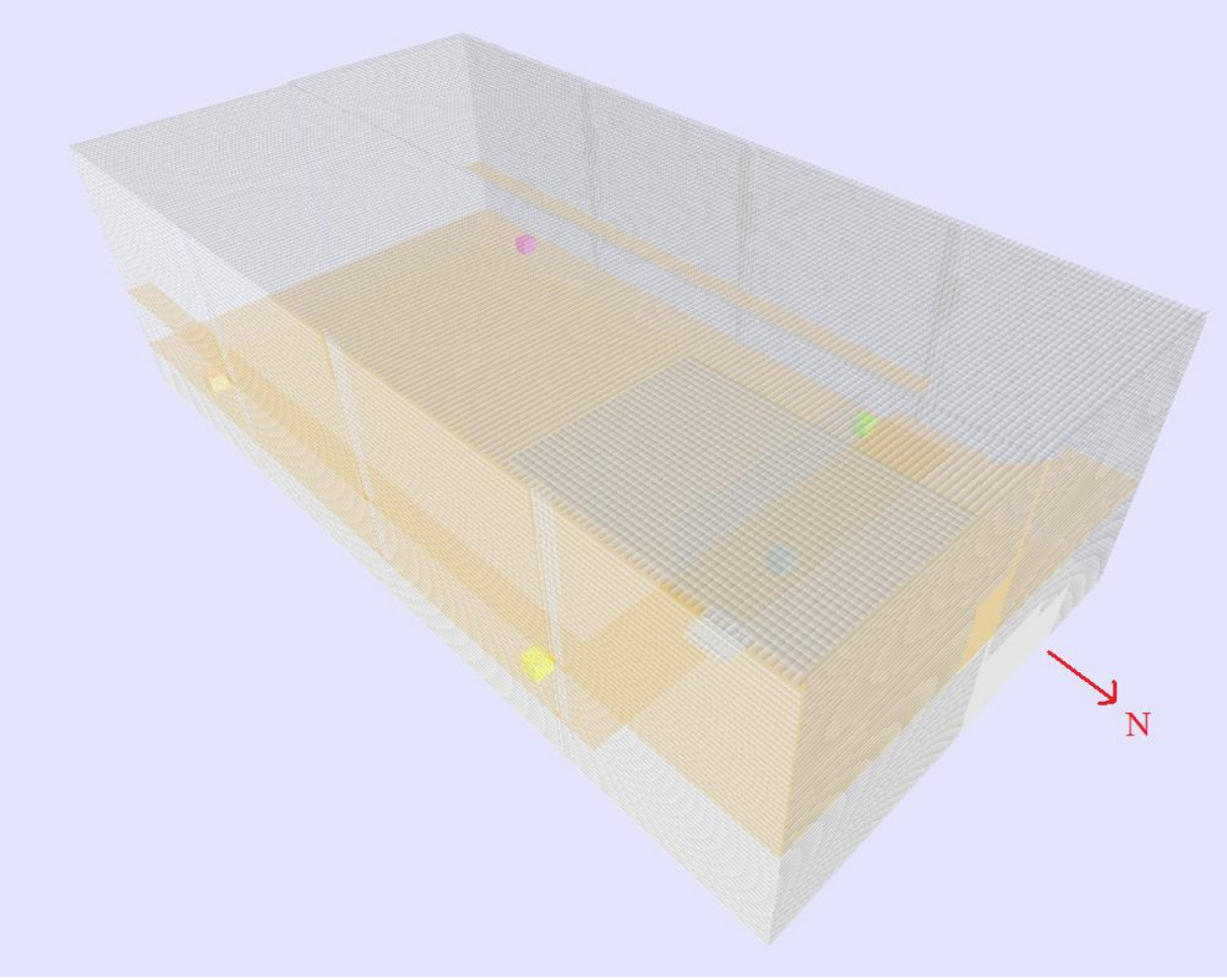

Figure 4. View of the vetoshield using the GUI.

The differential signals from the preamps are routed to the DAQ by means of 64 pin twisted pair cable. Each channel requires 2 lines on the cable for the differential signal and each tube has 2 channels, so each 64 pin cable can accommodate 16 tubes. The wall panels require 3 and a partial cable each and the ceiling panels each require 10 and a partial cable. There are additional extra cables for gap filling panels and other extra tubes. All of these cables are routed to four different racks containing the DAQ equipment. Each of these stations has cables routed to them such that each station roughly controls one geographical quadrant of the shield. Because of slight overloading of the northeast station will require extra DAQ equipment.

2.2 Gas handling system

The gas handling and control system was originally designed at Oxford University for both the vetoshield and the proton calorimeter. The gas rack itself with the diagram on its front is shown in figure 5. Although the majority of the gas handling system was removed with the calorimeters, the portions required for the operation of the vetoshield are still in place. Each tube is filled with a 90/10 Ar/CO_2 gas mixture which circulates through the tubes a few hundred mbar above atmosphere. The gas distribution system starts with the supply manifold which distributes the gas through ½" to 1" copper pipes to the individual panels. The individual tubes are daisy chained in groups of four with gas coming into the first tube from the supply pipe and leaving through the fourth tube into a return pipe. A restrictor, a pipe with a very small needle running through it, is placed between the supply pipe and the first tube in order to ensure am even flow of gas to every set of tubes as well as negate any sudden leaks in one section from degrading the gas in another. Finally, the return pipes return the gas to the return manifold.

From the return manifold the circulation pump moves the gas from the tubes through a catalytic converter which removes any oxygen which may have leaked into the gas stream. A mixture of the basic 90/10 Ar/CO_2 with 4% H_2 is injected before the catalytic converter to allow it to remove the oxygen. The normal levels of hydrogen to maintain in the system are on the order of 1000 ppm H_2. The hydrogen and oxygen levels are monitored by a set of sensors both before and after the converter which allow the amount of hydrogen required to be estimated and the efficiency of the conversion to be logged. The oxygen sensors also serve the function of stopping the circulation pump if the oxygen levels spike representing a major leak into the system. This is a crucial function given that it can take two to four

weeks to purge a contaminated panel completely. After the gas passes through the catalytic converter it travels back to the supply manifold.

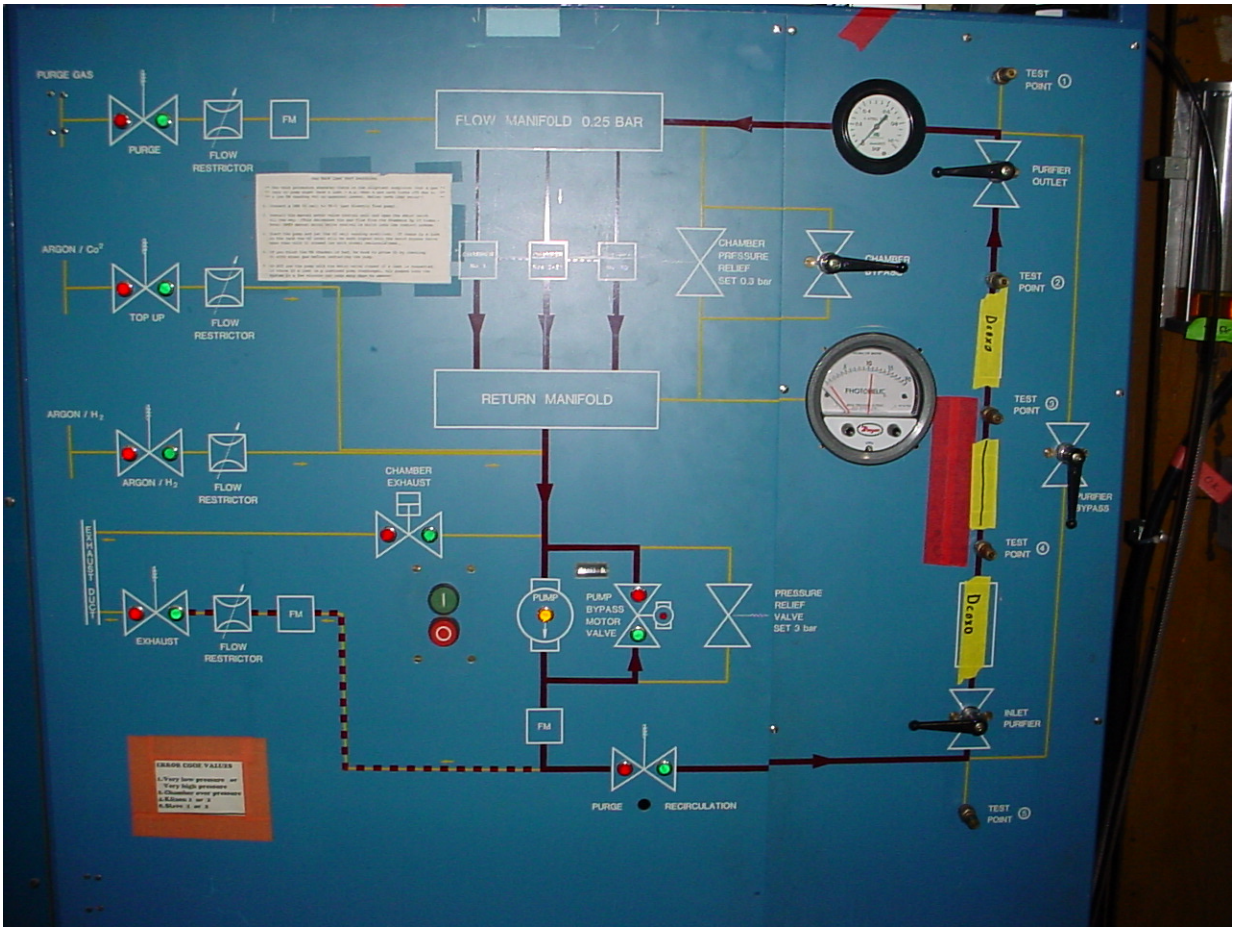

Figure 5. This is the gas rack which circulates the gas through the system and removes oxygen. The diagram on the front gives a good overview of the gas system.

Fresh gas to replace any gas that may have leaked out of the system is provided by a gas mixer which mixes the 90/10 Ar/CO_2 from bulk argon and carbon dioxide. The gas mixer used a differential regulator to equalize the pressure of the constituent gases and then combines the gasses through a disproportional number of equal area tubes; say 9 for argon and 1 for CO_2 (the actual number differs from this). The mixer creates the gas in batches and stores it in a large tank for use in the shield, these large batches help maintain consistency in the gas batches. New gas is mixed anytime the bulk mix tank falls below the lower pressure threshold. This gas is then injected into the supply manifold as necessary to maintain the proper pressure in the manifold.

2.3 Gas control system

The entire gas system is controlled by hardware which is original to the Oxford designed system, but it is being supplemented by a computer monitoring and control interface. The original control system used the information from the oxygen and hydrogen sensors as well as pressure sensors in the supply and return manifold to control the system. The oxygen and hydrogen sensors control the amount of hydrogen that is injected into the system in order to suppress all the oxygen in the gas. The pressure sensors in the manifolds are used to maintain the flow of the gas through the system. The gas control accomplishes this by opening or closing a bypass valve around the pump which increases or decreases the efficiency of the circulation pump as well as adding more fresh gas from the mixed any time the total system pressure drops below the set threshold of about 100+ mbars above atmosphere. There is a built in mechanical safety which stops the difference in pressure between the supply and return manifold from exceeding 0.3 bars. This slight overpressure keeps oxygen out of small leaks without having the added problems associated with higher pressures.

This system is being supplemented by a computer monitoring and control interface. The computer system will monitor all the quantities available to the old hardware control system as well as information of the temperature of the gas leaving and entering the pumps, the status of the main control valve, gas purity sensors, as well a sensor that monitors the percentage CO_2 in the gas coming from the mixer. The computer system will log these values as well as add new control options. The hydrogen levels will now be controlled in the computer allowing more dynamic control over hydrogen levels, but the pressure controls will be left under command of the original hardware setup. The computer has the ability to stop the circulation pumps if it detects any drop in gas quality in order to stop bad gas from flowing into the tubes. The computer also has the ability to stop gas coming from the mixer if it detects its quality drop below acceptable levels.

Chapter 3

Data Acquisition System

3.1 DAQ introduction

Unlike the other components of the vetoshield that have simply been refurbished and augmented, the data acquisition system has been completely replaced with a new system build from the ground up for use in the low background counting facility and its user oriented environment. The old CAMAC based DAQ system was simply too outdated and rigid for modern needs. The LBCF needed a DAQ system that could change to meet the needs of users in the LBCF at any particular time. To accommodate the different needs of many users at the same time as well as accommodate changes in requirements over time, we have based the design of this new DAQ around the use of complex programmable logic devices (CPLDs). These devices allow us to create a hardware design as general as possible and use the reprogrammable logic to modify the specifics of the logic function, and triggers of the shield as needed. The DAQ design has gone through 2 generations. The first generation was designed as an intermediary step to get data from the shield. The second generation was designed with the full use of the LBCF in mind and was base on CPLDs. Although the newest generation DAQ is of greatest interest, I will also explain the older DAQ system because the data presented in this thesis was acquired with this setup.

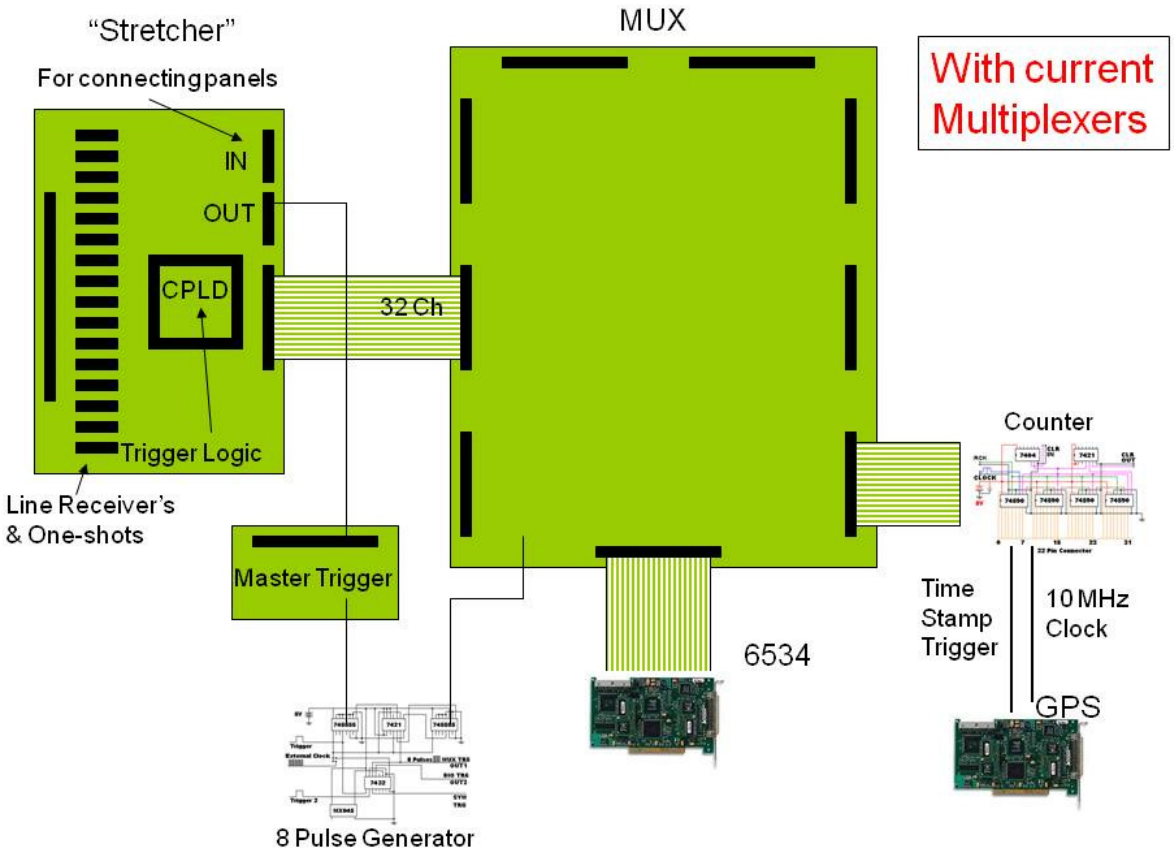

Figure 6. This diagram shows the individual cards required for proper operation of the first generation DAQ as well as their interconnections

3.2 First generation DAQ

The first generation DAQ, shown in figure 6, is based around two stages of processing: triggering and multiplexing. Each of these stages is carried out in a separate board. The first board is the pulse stretcher board. These boards each accept a single 64 pin (32 channel) signal cable and convert the signals from the differential pulses that preamps send out into TTL levels. The TTL level signals are then stretched from 1.2µs to 4µs with non-retriggerable one-shots to account for drift time in the tubes as well as other timing delays in the DAQ and cabling. From here the signals then travel into a Xilinx XC9572 CPLD where all of the trigger logic is implemented. Implementing the logic in the CPLD, as opposed to fixed logic, allows us to implement a wide and dynamic array of trigger choices. The CPLDS also allow easy implementation of triggering schemes that would be unpractical in traditional logic. On

the pulse stretcher the trigger is delayed by 1.5 μs in order to make up for differences in drift time between tubes.

From the pulse stretcher the stretched pulses are sent to the multiplexer board by means of 34 pin ribbon cable. The multiplexer board multiplexes between eight different stretcher boards and send this information to the computer DAQ card. The first generation multiplexers are implemented with standard TTL logic chips and are controlled by a single clock input. In order to make the DAQ read once from each stretcher a small supplemental board was built to take the triggers sent from the pulse stretcher boards and repeat it 8 times at 10 MHz.

This eight pulse train caused the multiplexer to switch once on the rising edge of each pulse and the National Instruments 6534 DAQ card in the computer to capture the data on the falling edge. The 10MHz clock was chosen so that the read of all 8 channels plus the 1.5 μs delay in the trigger are all done before the 4 μs stretches in the signals are over. This assures that we do not lose any data to either drift time delays or to pulses dying out before we read. The final part to the first generation DAQ design was a modification which allowed the data to be time stamped. We created another supplemental board which included a 32 bit counter which we clocked with the same 10 MHz signal as the DAQ read. This board then replaced one of the pulse stretchers on the multiplexer board and allowed us to timestamp the events with the counter value. This relative time stamp was converted to an absolute timestamp by means of the Symmetricom GPS card. The GPS card provided the 10 Mhz signal as well as a timestamp for the start and reset of the 32 bit counter that are synchronized to the GPS time feed in Soudan.

This DAQ setup allows for correct acquisition of data but with a minimum of adaptability. The pulse stretcher design is good with the adaptability of the CPLD trigger logic, but they have minor flaws such as the non-retriggerable one-shots which cause a small fraction (~0.5%) of events to be missed. The multiplexer on the other hand is completely unacceptable for the purposes we need to put it to. Its lack of programmable logic and inability to apply timestamps or control the read without additional boards makes it unsuitable for the LBCF. This requirement for the external timer also takes a slot away from pulse stretchers only allowing 7 stretchers per multiplexer instead of 8.

3.3 Second generation DAQ

The second generation DAQ setup, shown in figure 7 & 8, is designed to integrate all the individual components of the prior DAQ and improve upon its design. Like the first generation DAQ the

current design is based around the two primary steps of triggering and multiplexing. The pulse stretchers for the current design are similar to that of the old design. The one-shots are retriggerable in the current design. The pulse stretchers have also been modified so that they now plug directly into the multiplexer instead of through a cable. The final design change to the stretchers is to do the first phase of multiplexing in the stretcher CPLD to reduce the number of data lines in the multiplexer as well as the addition of data latches to the data lines. The controls for the multiplexers in the stretcher CPLD comes from the multiplexer board.

The new multiplexer is now implemented entirely with 3 Xilinx XC9572 CPLDs; one of the CPLDs serves as the controller for the data read and the other two handle the timestamp and second phase of multiplexing. The controller CPLD takes the triggers from each of the eight pulse stretchers and concatenates them. It then initiates the read by sending out the multiplexer control bits to the stretchers and multiplexer CPLDs and sending a read trigger to the NI 6534 DAQ card. Unlike in the old DAQ the trigger is delayed inside the trigger CPLD instead of using a one-shot. This allows us the freedom to change the delay as necessary without having to replace physical components.

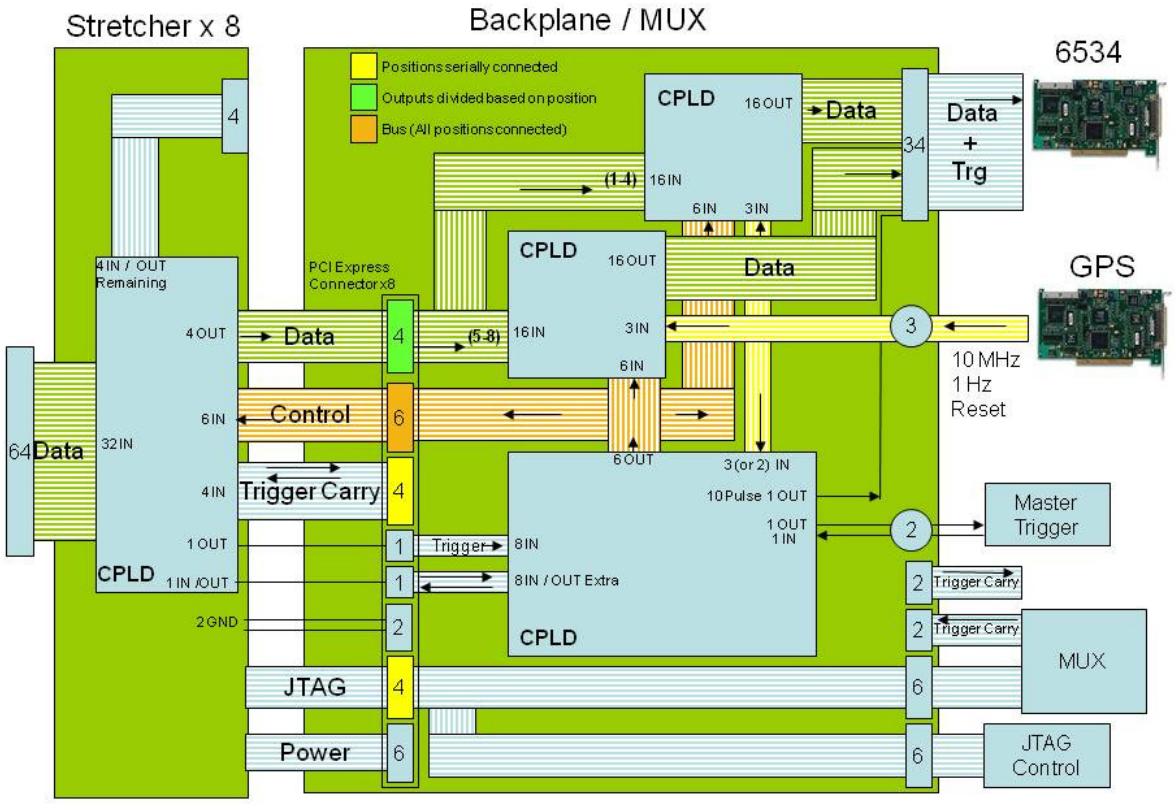

Figure 7. This is a schematic showing the components and interconnections on the second generation of the DAQ.

Figure 8. Front and read pictures of the second generation DAQ being tested at the University of Minnesota.

The multiplexer chips each multiplex the data from four of the eight stretchers. The multiplexer CPLDs also contain a 1 Hz and a 1 MHz counter which are clocked off a 5 Mhz and 1 Hz signal from the Symetricom GPS card. These two GPS synchronized counters allow accurate timing of the events to within ±2 μs due to drift time. The use of both the 1 Hz and 1 MHz counters allows us to run for up to 136 years before we have to worry about timer flips. These counters are split between each of the two multiplexer CPLDs and are multiplexed into the data read at the end of the data read along with a fixed string which is used to check for DAQ read errors and another string which reports whether or not each stretcher is plugged in and operating.

3.4 DAQ Timing

Both the first and second versions of the DAQ use NI 6534 card to read in the information into the computer. The 6534 card reads data at the request of the DAQ as described above. The DAQ multiplexes through the data and requests the 6534 to read once for each data set. With the first

generation DAQ the 6534 does 8 reads in 800 ns to read in all the required data. The second generation DAQ requires 12 reads over 2.4 μs, but the addition of the data latches to the current design stops the chance of losing any data. The total DAQ timing sequence starts with the signal in the preamp which travels to the stretcher board. Here the trigger logic may or may not be triggered. If the trigger is sent out, it then travels into the multiplexer board where it will trigger the start of the read. The read begins with a 1.2 to 1.4 μs (6 or 7 clock cycles of the 5MHz clock) delay to wait for any signals which may have had longer drift time. After this delay the read controller starts the multiplexers switching and cause the 6534 DAQ card to read twelve times, once for each of the eight stretchers, the stretcher info line, the two counters, and finally the error checking line. For the entire 12 clock cycles of the data read (2.4 μs) the data is latched in the stretchers to stop the remote possibility of signals dying out before they are read or the more likely case of new noise signals showing up that are not part of the event of interest. The timing of the DAQ is summarized in figure 9. The entire read starting from the beginning of the decay and extending two clock cycles past the end of the data read is enveloped by a non-retriggable window. This window lasts 4.0 to 4.2 μs from the trigger to the time another trigger can activate another read. The tail after the end of the read accommodates for the possibility of the trigger still being high after the end of the read because of the drift time delayed signals. This window gives a maximum data rate for the DAQ to be 238 KHz which is far above the faster data rate that can be achieved under normal operation of full multiplexer containing 256 data channels (8 stretchers with 32 channels each). Because of the 4 μs stretch in the signals in the pulse stretcher, it is not possible to cycle the trigger faster than 250 KHz at an absolute maximum.

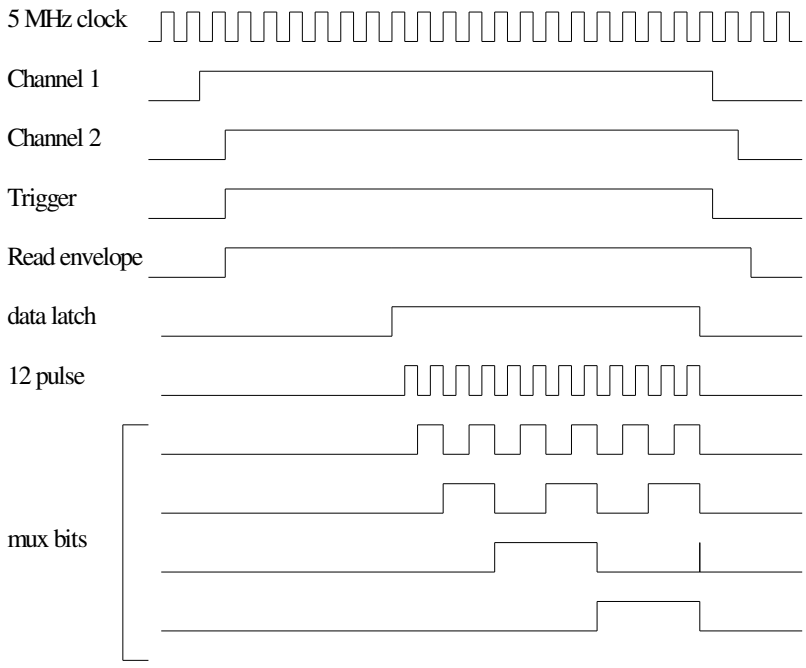

Figure 9. Timing diagram for the DAQ. Here Channel 1 and 2 are represent two channels on a pulse stretcher representing a coincident. The difference in their timing is drift time difference.

With each multiplexer board able to accommodate 8 pulse stretchers and each computer able to accommodate 2 NI 6534 cards (each which can handle only one multiplexer), we are able to accommodate a total of 16 64 pin signal cables with a single computer. This means that there need to be a total of five computers to take data for every channel of the vetoshield. As described above there are four stations to which the signal cables are routed. Each station has one computer except for the northeast station which will require two. The data from the five individual computers will be sent to a central data server where all the users of the LBCF will have access to it.

3.5 DAQ software

We use a program written in LabView, shown in figure 10, to read the data from the NI 6534 card into the computer. This program is setup to read the data in and reconstructs it before it is saved into file. The reconstruction is necessary because the first phase of multiplexing causes the data to me mixed in an unintuitive way. Once the data is reconstructed it can be saved directly to file or stored in a database for later use. Beyond simply recording the data, with the current DAQ software we also check for errors such as the 6534 buffer or the timer getting out of sync and are able to reset the read in these

cases. Although these problems should be very rare they are possible and we can stop them from getting worse by detecting and stopping them.

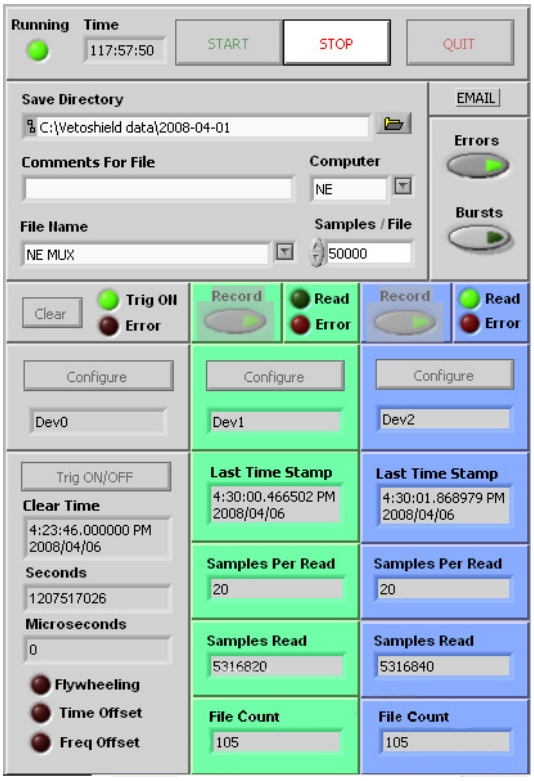

Figure 10. This is the LabView program used to take data from the DAQ.

There is also a diagnostic data taking program which simply displays the data directly on screen and bypasses writing it to file. This allows us to get real time responses for testing the DAQ and the tubes themselves. This program will either display the direct binary representation of the data coming out of the DAQ or it will operate in a scalar counting mode and simply count the number of hits received on each data channel over a specified period of time. The scalar count mode can then be displayed a chart form to compare the channel performance. A second diagnostic program has been written as well to test the entire DAQ. This program uses a 32 channel switch box to represent data coming from a preamp card and can sweep through any combination of channels to ensure that the data is being displayed in the correct places and that the triggers are going off under the correct conditions.

3.6 Trigger configuration

The biggest advantage to designing the DAQ with CPLDs is that the trigger logic can be made more advanced without requiring large number of chips as well as the logic can be changed at any time to meet the needs of the LBCF. The basic trigger logic for the vetoshield is based on the idea that there

have to be at least two channels high in order for us to consider the event a muon: furthermore, we took advantage of the overlapping nature of the veto tubes to limit the trigger rate to the minimum possible. This is accomplished by a triggering scheme where each channel may trigger with the other channel on the same tube or with either of the two channels across from it on adjacent tubes. This triggering scheme is illustrated in figure 11. With this triggering scheme we are able to trigger on muons coming at any angle or location through the shield and we do not trigger on any events that clearly are not muons. This scheme is implemented inside the CPLDs on the pulse stretcher boards. There are interconnects between stretchers which allow the last channels of one stretcher and the first of the next stretcher to trigger each other in this same way so there are no gaps between cables. We are also capable of adding more or less strict triggers by simply changing the logic in the CPLD. For instance it may be desired that all events regardless trigger a data read, or it may be required that two layers of tubes have muon hits at the same time. These cases as well as many more are possible with the CPLD logic. A board can be left without trigger logic and simply be used to read data in a slave mode as well.

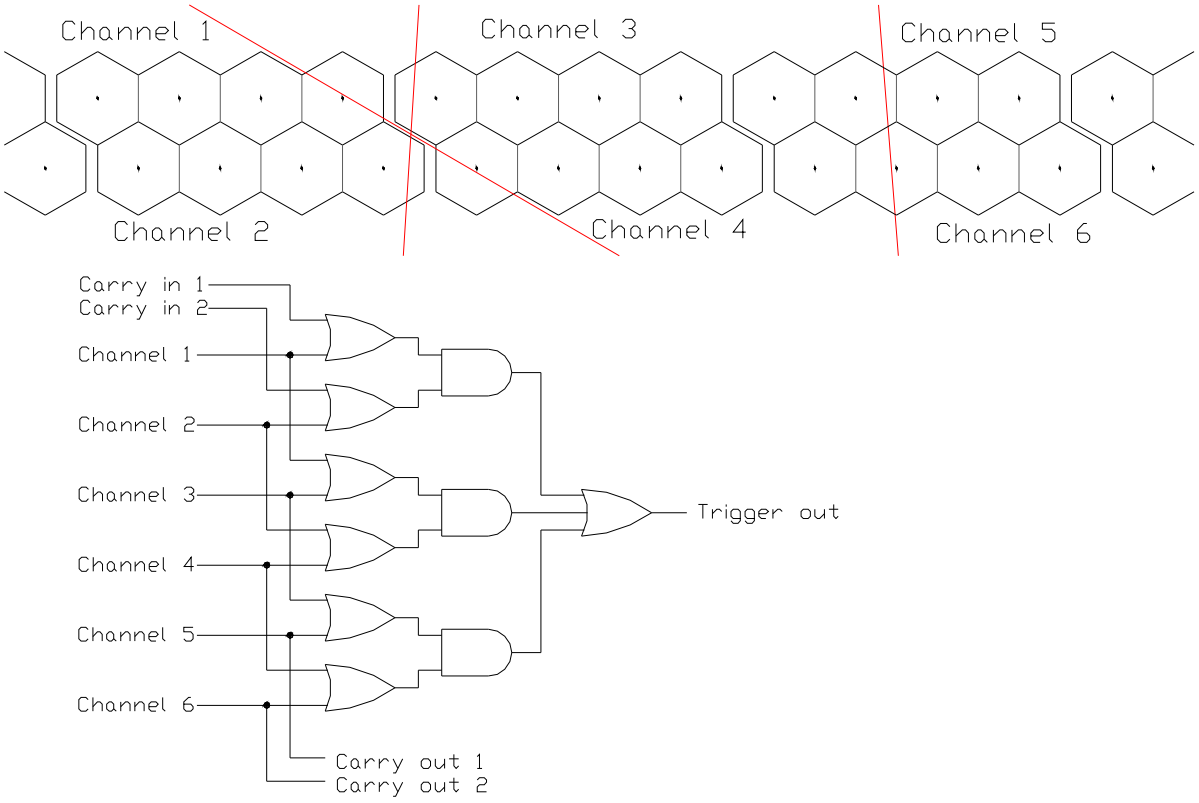

Figure 11. This is an illustration of our primary trigger logic implemented for three tubes. The three possible path types that can cause a trigger are shown in red. The logic implementation is also shown for this three tube system. The carry in and carry out bits allow the logic to be linked in between stretchers.

This flexibility in the programming of the trigger is further augmented with the ability for the multiplexers or stretchers to send or receive external triggers. Each of the ten multiplexers required to operate the vetoshield will have its external trigger in and out connected to a central trigger control box. This box will contain a CPLD each to control the input and output triggers and will have a number of trigger in and out lines which can be used by users to either receive a veto pulse from the shield or to send out a trigger to cause the shield to read. Because the shield is spread over ten multiplexers and these multiplexers each are generally localized to a general geographic region, the CPLDs can be programmed to give a localized trigger to meet user needs. Some users may need access only to a small portion of the shield, while other users may require access to the entire shield. With the use of programmable logic here we can meet the needs of every user individually. If any user should require even more localization we can provide them with access to the trigger coming from a single pulse stretcher by means of an extra output designed into the stretchers. This system gives a flexible user oriented system which should be able to deal with the changing environment of the LBCF.

3.7 Veto tube efficiency

In order to measure the muon detection efficiency of the tubes, we have taken a number of tubes from the lab and brought them above ground at the University of Minnesota. The above ground stack of tubes gives us the muon flux to be able to measure the efficiency precisely in a reasonable amount of time. The stack is setup so that there are five stacks of three tubes each, one on top of the other. We then take data triggering in a mode which required both the channels in both the bottom and tube to be high. If the muon passed through both the top and bottom tube we know it must have passed through the middle tube, so the efficiency is calculated by taking the number of events that trigger all three tubes divided by the number which only triggers the top and bottom tubes of the stack. This is found individually for all five stacks of three tubes and averaged to find the average efficiency of the veto tubes. Found with the first generation DAQ, the maximum in efficiency is 98.8 ± 1% takes place around 2400 V. The entire platue is shown in figure 12 along with the counting rate for a single channel. This is in line with the expected result for the maximum efficiency of >99.5% which was the claimed efficiency during running of the Soudan II experiment. It is possible that the use of the first generation DAQ system with non-retriggerable one-shots has caused a shortfall in the efficiency of about 0.5%. There is also a slight mismatch in the lengths of the tubes which is on the order of 1%. If these factors were corrected for it is likely we would find an even higher efficiency.

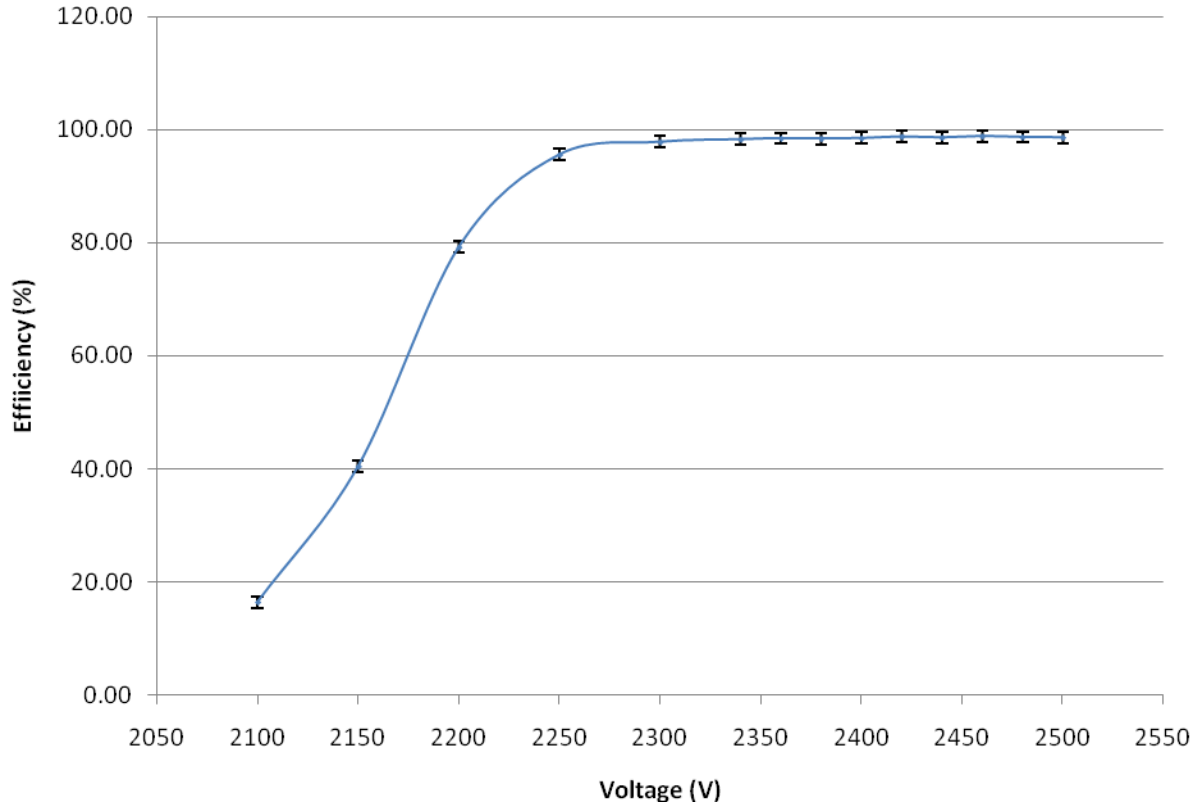

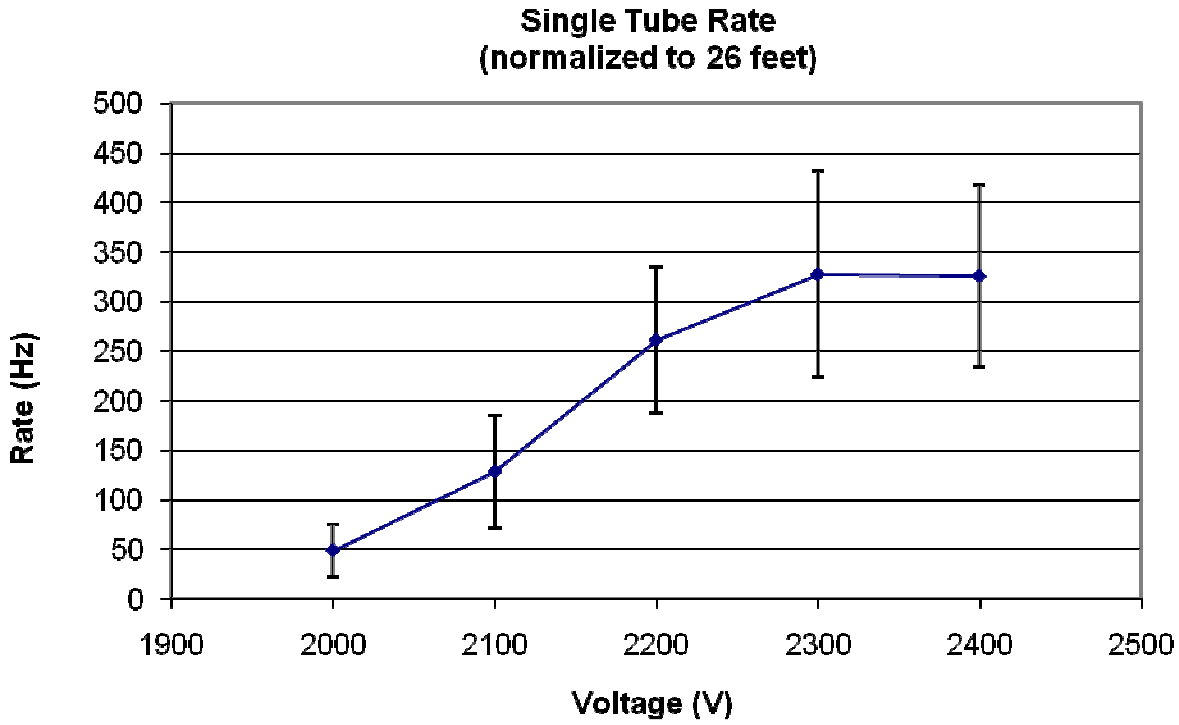

Figure 12. On top is an efficiency platue for the above ground tube stack. On the bottom is the counting rate for a full length 7m tube.

Chapter 4

Angular distribution measurements

4.1 Angular measurements

The angular distribution at the Soudan Laboratory is an important piece of information for the characterization of the environment in the LBCF. These measurements also serve as benchmark for the Monte Carlo generated muon distributions. These distributions are generated by the Music code and are then used to simulate more elaborate simulations with different Monte Carlo codes. These data can ground the simulations [4]. Finally, these measurements serve as a demonstration of the functionality of the vetoshield.

All the data for the angular distribution were taken with the Soudan LBCF vetoshield using the first generation DAQ. The data was taken over 6 months from August 2007 to February 2008. The DAQ was taking data non-stop for entire time with the exception of downtime for repairs, mostly due to the gas system. The total data acquisition time was 2163 hours.

4.2 Experimental setup

The data were all taken in the NE corner of the LBCF hall where the new clean room is now located. This location is optimal for these calculations because, as mentioned before, there is a second layer of crossed tubes over the clean room to provide better paths through the clean room. The second layer on the tubes of the ceiling contains 29 tubes each seven meters long. This gives an area of 7 meters by 5.5 meters of detector area which is entirely covered below by tubes from the regular ceiling.

These two orthogonal layers of tubes allow us to localize the muon paths accurately to the width of a tube (19 cm) in the x and y directions and to the height of a tube (8 cm) in the z direction.

The ceiling tubes are supplemented with a small stack of tubes, the test stack, placed below the ceiling in the clean room. The test stack is located about 4.8 meters below the ceiling on the raised mezzanine above the primary floor. The stack itself contains 16 tubes each of about 1.4 meters long which are assorted in three layers. Unlike the stack used to calculate the efficiency of the tubes, these tubes are arranged so that the top and bottom layer each contain 5 tubes running in the same direction and 6 tubes in the center running in the opposite direction. This configuration allows the location of the muon track in the same way as in the ceiling. This test stack combined with the ceiling gives us two points from which to calculate both the zenith and azimuthal angles from.

Despite being on the second level, to be as close to the ceiling as possible, the maximum angle that can be covered by this setup is still only about 37° of coverage in zenith angle. In order to increase this range further, we are able to include data from the adjacent panel on the east wall. By taking a hit in the test stack and the wall we are able to calculate its zenith angle, though the lack of a second layer of orthogonal tubes on the walls precludes the measurement of the azimuthal angle from this data. The wall panel comes 40 cm below the ceiling panel on the top and goes all the way to the floor. Because the test stack is positioned about half way up the wall, it can provide zenith measurements for the wide angle muons in both the east and west directions. Unfortunately, the north wall is not in sufficiently good working condition to make similar measurements in the north-south orientation.

The criterion for the angle muons was set before the beginning of the experiment to be an event which there was a hit in both layers of the ceiling and a hit in at least two orthogonal layers of the test stack for the narrow angle events. An angle event is shown in figure 13. For the wide angle events the requirement was that there are at least two hits in orthogonal layers of the test stack and one hit in the wall. When I use the word hit I refer to either both channels of a tube going off at the same time or a channel in one tube and the opposite channel in an adjacent tube going off at the same time. In either set of data an event is discarded if there is any ambiguity in the path of the muon because there is no way with this detector to tell which of a number of paths might be the true path.

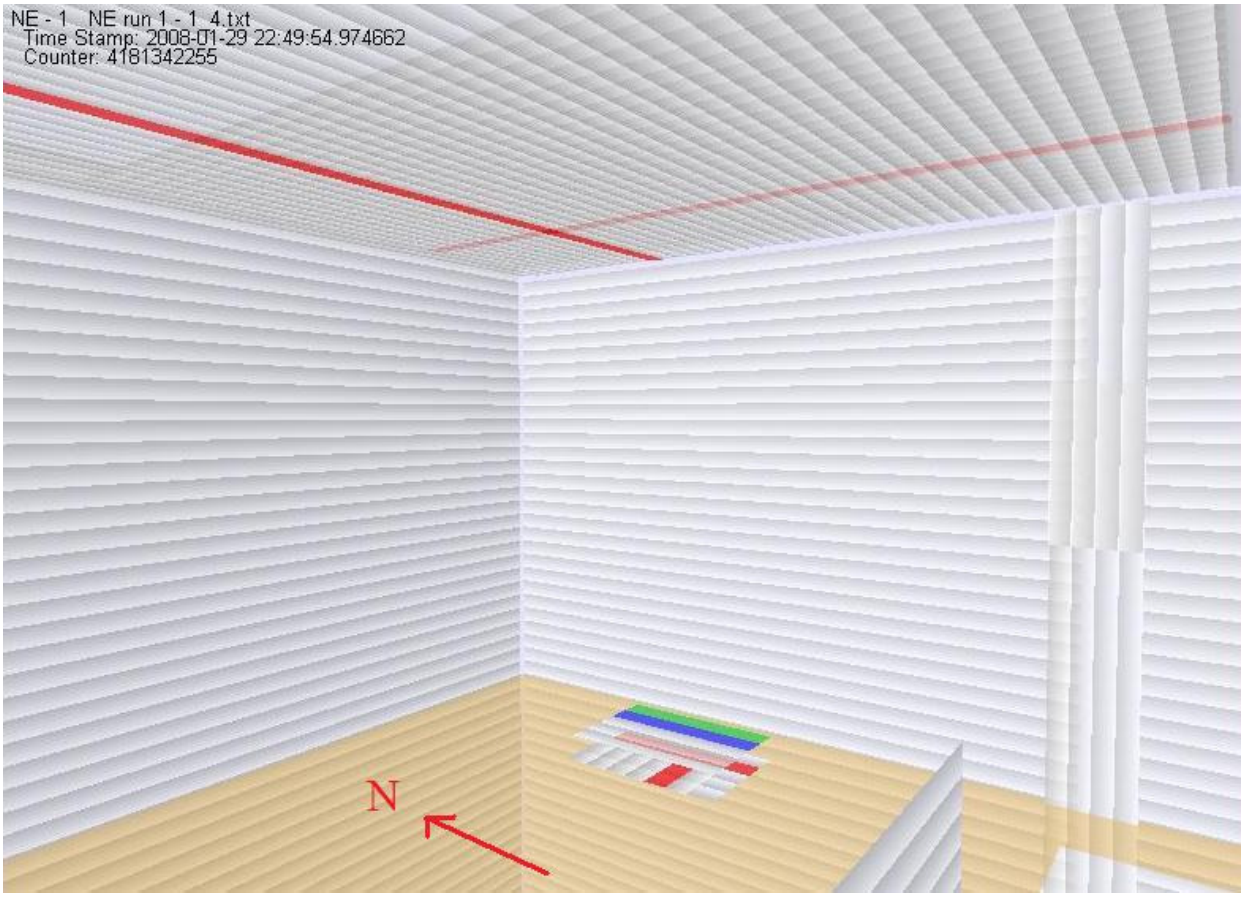

Figure 13. This is an angle event shown in the GUI. There are 2 events in the ceiling and 3 in the test stack. The red color indicates the inner are outer channel on a tube are both hit. The green and blue mean the inner or outer have been hit.

We choose to trigger all this data with the test stack alone in order to get data with both the walls and the ceiling. We did not trigger on other panels because the first generation of the DAQ was not reliability capable of triggering off more than one panel at time. We choose the hardware trigger for the test stack to be the G2 trigger discussed in the trigger section above. This triggers if both channels in a tube or a channel and the opposite channel in an adjacent tube go off at the same time. This trigger in the test stack yields a trigger rate of roughly 10 Hz. We could have implemented a tighter trigger because of the requirement that there be hits in at least two layers of the test stack's three layers, but we wanted to keep the trigger as loose as possible so other information can be extracted from it while the 10 Hz rate keeps us from taking more data than we and the old DAQ can handle.

4.3 Angular distribution decomposition

The format of the raw data is simply a list of eight unsigned integers per event where the first seven integers represent the high channels on each stretcher and the last integer represents the time elapsed since the beginning data run. These files in themselves do not contain any information about the location of the events. The location is instead held in a survey file which was made from the initial survey of the tube positions during their installation during Soudan II construction. This database contains the location of every panel which was installed during Soudan II construction to within a few centimeters. The second layer on the ceiling and the test stack were added later so their locations were measured with respect to preexisting panels.

The analysis code, written in Java, is provided with a map which connects the columns in the data files to physical panels whose locations are known. It then processed all 84.5 million events and used a software trigger to filter out the events which conform to the restrictions on an angle event described above. For events that match the conditions to calculate the angles, the x, y, z coordinates in the test stack and wall/ceiling are calculated. In the ceiling the location is found by locating the spot where the two tubes with hits intersect. The intersection point is simply found by taking the north-south(x) position of the tube running in the east-west (y) direction and the east-west coordinate of the tube running in the north-south direction. The height coordinate (z) is simply found by averaging the height of the tube in the ceiling and second layer which is a constant in the ceiling.

The calculation in the test stack is a little more complicated because there are three layers instead of two, but the general approach is the same. When there are hits in only two layers there the method is exactly the same, but when all three layers are hit the x coordinate is calculated in the same manner, but there are now two tubes to get the y location from. This problem is overcome simply by averaging the y location between the two tubes if more than one is hit for the event in question.

The calculation of position for wall events posed a different problem. With no second layer of tubes on the wall is only possible to know the y and z components of the x, y, and z position. In this case we simply choose to take the center of the tube as the x position of the tube but we cannot assume any precise knowledge in this direction.

Once we know the x, y, x positions in the test stack and wall or ceiling for each event we can calculate the azimuthal angle (θ) and the zenith angle (ϕ). Basic trigonometry tells us that

$$\phi = \arctan\frac{\sqrt{\Delta x^2 + \Delta y^2}}{|\Delta z|} \tag{1}$$

In this equation Δx, Δy, and Δz are the difference in the x, y, and z components between the wall/ceiling location and the test stack location. The value of ϕ in this equation is limited to the range 0 to π/2 where 0 is a completely vertical. The azimuthal angle can be found similarly as

$$\theta = \arccos\frac{\Delta y}{\sqrt{\Delta x^2 + \Delta y^2}} \tag{2}$$

Again Δx and Δy are the difference in the x and y components between the wall/ceiling location and the test stack location. The range of the azimuthal angles is -π to π where zero corresponds to due north.

4.4 Angle error analysis

The error in the measurements of the angles comes primarily from the size of the tubes and the error in their location. The error in the measurement of the position of the tubes is on the order of a few centimeters but it is not known what the exact tolerances of the measurements were. The size of the tubes on the other hand is known to be 19 by 8 centimeters. The length of the tubes is irrelevant because the tub's length is never used. The error due to the width of a tube is therefore ±9.5 cm and the approximate error in the measurement is about ±2 to 3 cm so the total error is ±10 cm. In the case of the x measurement we have 2 tubes and the error is there ±8 cm with an additional error of about 2 or 3 cm which gives an error of ±8.5 cm. In both cases the error introduced because of the uncertainty in the location of the tubes is small compared to the width of the tube. The uncertainties in the original measurements are also reduced because the second layer and the test stack were located with respect to the ceiling. This makes the absolute error greater, but our measurements only care about relative measurements in location causing absolute measurement errors of these panels to cancel.

The formula for the errors in the azimuthal angles can be calculated from the equations (1) using standard error propagation as follows

$$\sigma_\theta = \sqrt{\frac{\Delta y^2 \sigma_{\Delta x}^2 + \Delta x^2 \sigma_{\Delta y}^2}{(\Delta x^2 + \Delta y^2)^2}} \tag{3}$$

In this equation σ_θ, $\sigma_{\Delta x}$, $\sigma_{\Delta y}$ are the uncertainties in θ, Δx, and Δy respectively. The error in the zenith angle can similarly be found from equation (2) to be

$$\sigma_\phi = \sqrt{\frac{\Delta x^2 \sigma_{\Delta x}^2 + \Delta y^2 \sigma_{\Delta y}^2 + (\Delta x^2 + \Delta y^2)^2 \sigma_{\Delta z}^2}{(\Delta x^2 + \Delta y^2)(\Delta x^2 + \Delta y^2 + \Delta z^2)^2}} \tag{4}$$

In the above equation σ_ϕ, $\sigma_{\Delta z}$ are the uncertainties in the measurements of ϕ and Δz respectively. Using the value for z = 484 cm, the distance between the test stack and the ceiling, $\sigma_{\Delta x} = \sigma_{\Delta y} = 10\sqrt{2}$ cm = 14 cm, and $\sigma_{\Delta z} = 8\sqrt{2}$ cm = 11 cm the zenith angle and its uncertainty are plotted in figure 14 over the range of interest with y = 0.

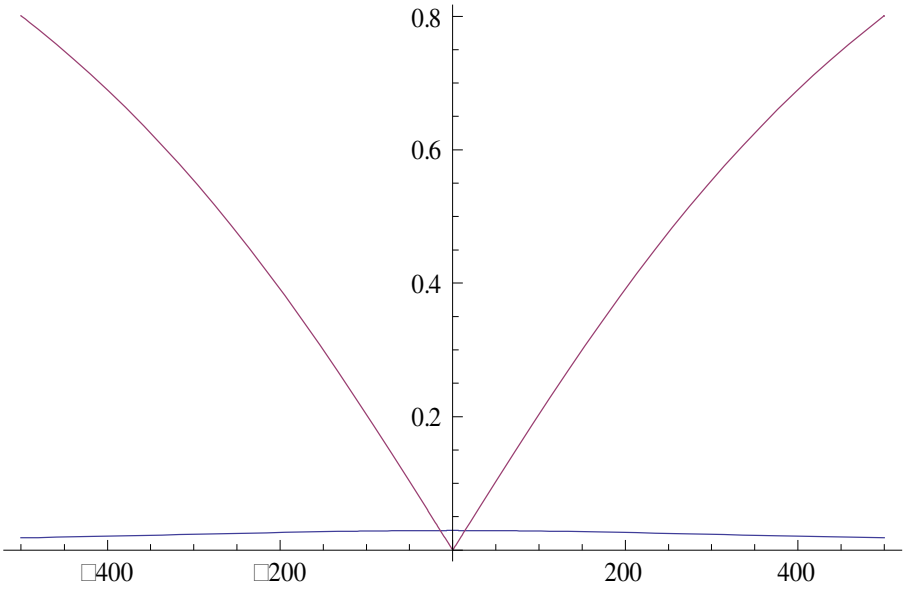

Figure 14. This is a plot of the zenith angle and its statistical error as a function of Δx (or Δy). The red curve is the angle and the lower blue curve is the statistical error.

Equation (4) works well for the uncertainties of the measurements of the zenith angle between the test stack and the ceiling, but it breaks down in the measurements involving the wall and the test stack. The inability to give the hit a concrete location in the x direction on the wall causes a huge asymmetry in the uncertainties with a 19 cm width in one direction and a 700 cm length in the other. If we try equation (4) with $\sigma_{\Delta x}$ = 350 cm we find that the uncertainty in σ_ϕ becomes very sensitive to the value of Δx, but the value of Δx is not known well so it does not make sense that the uncertainty should depend so strongly on it. To overcome this problem in the standard error equation we have to give up any azimuthal information (which we already have to do anyway) and only look at the y and z dimensions of the data. The equation used in these cases is

$$\sigma_\phi = \sqrt{\frac{\sigma_{\Delta y}^2 + (\Delta x^2 + \Delta y^2)^2 \sigma_{\Delta z}^2}{(\Delta x^2 + \Delta y^2)(\Delta x^2 + \Delta y^2 + \Delta z^2)^2}} \qquad (5)$$

where the Δx is a minor adjustment for the misalignment between the center of the wall tubes in the x direction and the center of the test stack.

4.5 Azimuthal angle data

The Azimuthal measurement is made using the data from the ceiling, but in order to compensate for the rectangular shape of the ceiling we must make a cut on the zenith angle of the data. The zenith angle is limited to less than 0.5 radians which is the largest angle for which we can choose a circular region of the ceiling centered above the test stack. The azimuthal distribution found is shown in figure 16.

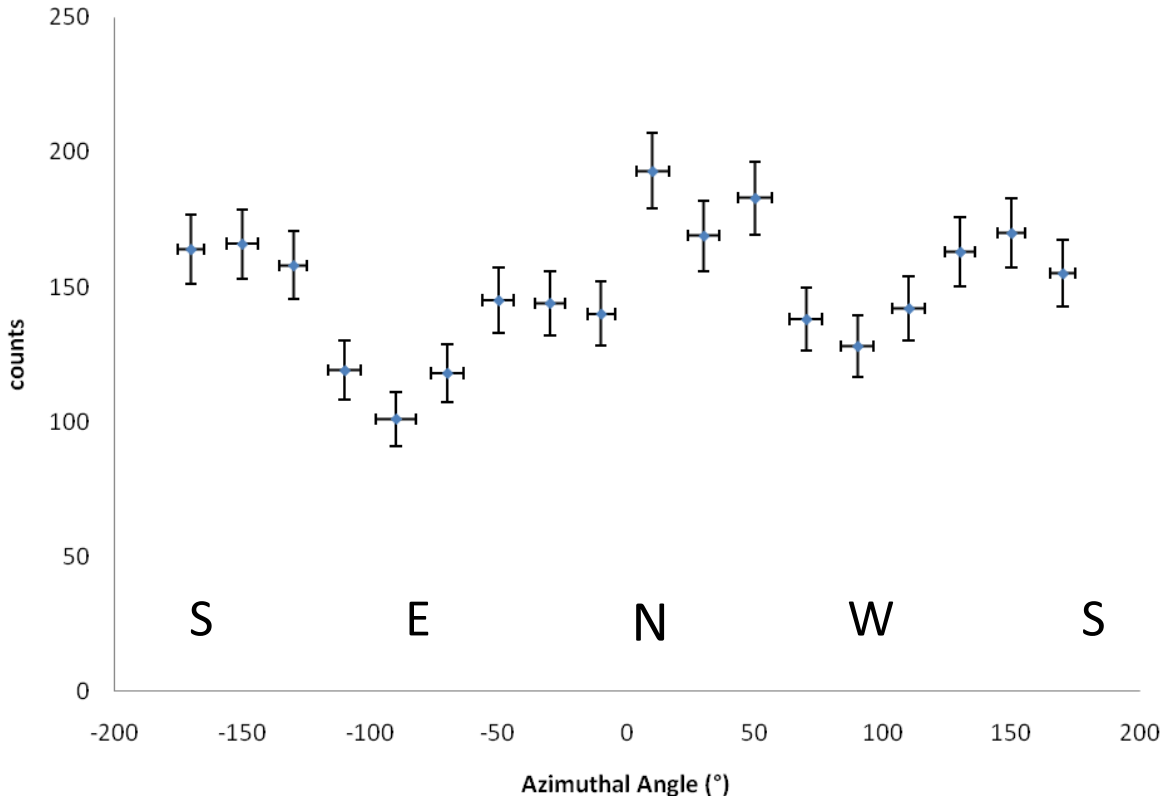

Figure 16. This is the plot of azimuthal angle as measured in the ceiling with zenith angle less than 0.50 radians. This plot contains a total of 2696 data points. The cardinal directions are marked.

Figure 16 shows a marked difference between the relative muon fluxes in the east-west and north-south direction. The due E-W flux is 30 ± 6% less than due N-S flux. This disparity in the relative flux rates can be explained by the geography of the laboratory. The Soudan Laboratory sits under a

ridge which runs in the east-west direction. This ridge lies about 70 meters above the ground to the north and 60 meters above the ground to the south, but the azimuthal angle data is limited and does not see this entire height difference. The remaining differences in the flux can be explained by the differences in the rock above the cavern. Although the laboratory itself is surrounded by Ely Greenstone, there are deposits of iron bearing taconite (~30% iron) around the now excavated hematite (~65% iron) which increases the density of the rock. These taconite deposits follow the east-west direction of the original iron rich veins so increasing the density of the rock above the laboratory in this direction [5]. The ridge can be seen running over the lab in figure 17.

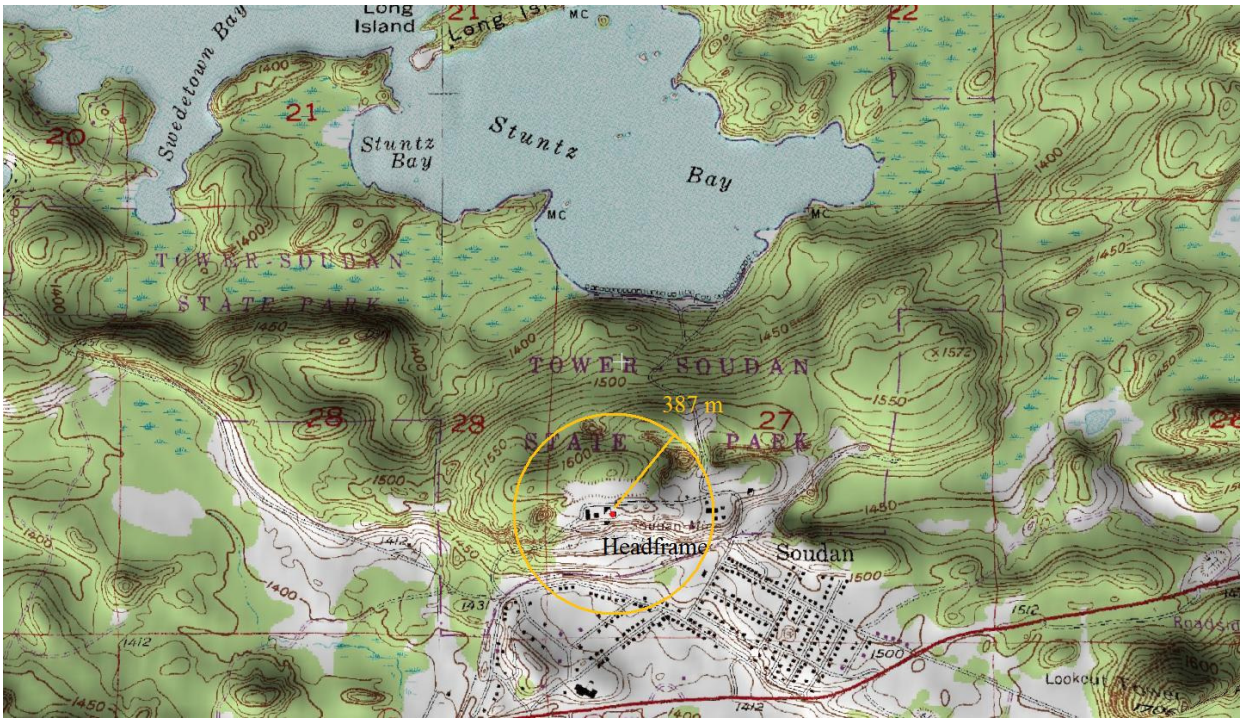

Figure 17. This is the topographical map of the area around Soudan. The red dot represents the location of the Soudan lab position. The yellow circle represents the projected area from which data is taken for the azimuthal plot. [6]

4.6 Zenith expectations

The basic method to parameterize the zenith distribution of muons is

$$P(\phi) = \cos^n \phi \tag{6}$$

where n is any real number greater than two. On the surface one would find n ~ 2 and it increases as you move underground. Of course there are bound to be deviations from such a simply

parameterization in this system. We have already seen that the azimuthal distribution is not uniform as well as seen that the overburden of the laboratory varies in rock density. To that end we expect there to be deviations from this basic distribution that will make a reasonable fit impossible, but we will see that the general shape of the distribution is not entirely divergent from such a fit.

In 2002 Robert Nelson of UC Santa Barbara used three sections from the CDMS vetoshield to measure $n = 3.28 \pm 0.13$. Nelson did not directly measure distribution but instead convoluted the value of n from a measurement of the energy of the muons. He also would have preferentially looked at more vertical muons because he required a coincident in all three of his scintillator panels. The distribution at Soudan does not necessarily follow the same distribution at narrow and large angles, none the less we will use his measurements as a starting place [7].

4.7 Zenith angle Monte Carlo

We chose to produce a simple Monte Carlo simulation to predict output of the zenith distribution from the vetoshield. The Monte Carlo was designed to simulate the geometry of the shield which is in use as well as the muon distribution, but it neglects any other factors that are beyond the ability of out instruments to measure (such as energy). The Monte Carlo starts by generating muons from a random location in the test stack and throwing them with an even azimuthal distribution. The zenith distribution on the other hand is generated to conform to the distribution in equation (6). The Monte Carlo then checks weather the generated muon passes through either the ceiling or the wall. If the muon passes through the ceiling, the zenith angle is simply recorded, but if the muon passes through the wall more must be done. If the muon passes through the wall then the zenith angle is recalculated using only the y and z data and the x position is discarded. This is done to accurately represent our ability to measure the angle using the wall. The distribution is equation (6) as seen in the wall section of the vetoshield is shown in figure 18 for various values of n. Figure 19 shows the difference in zenith distribution in the wall before and after correcting for the lack of knowledge in the x direction.

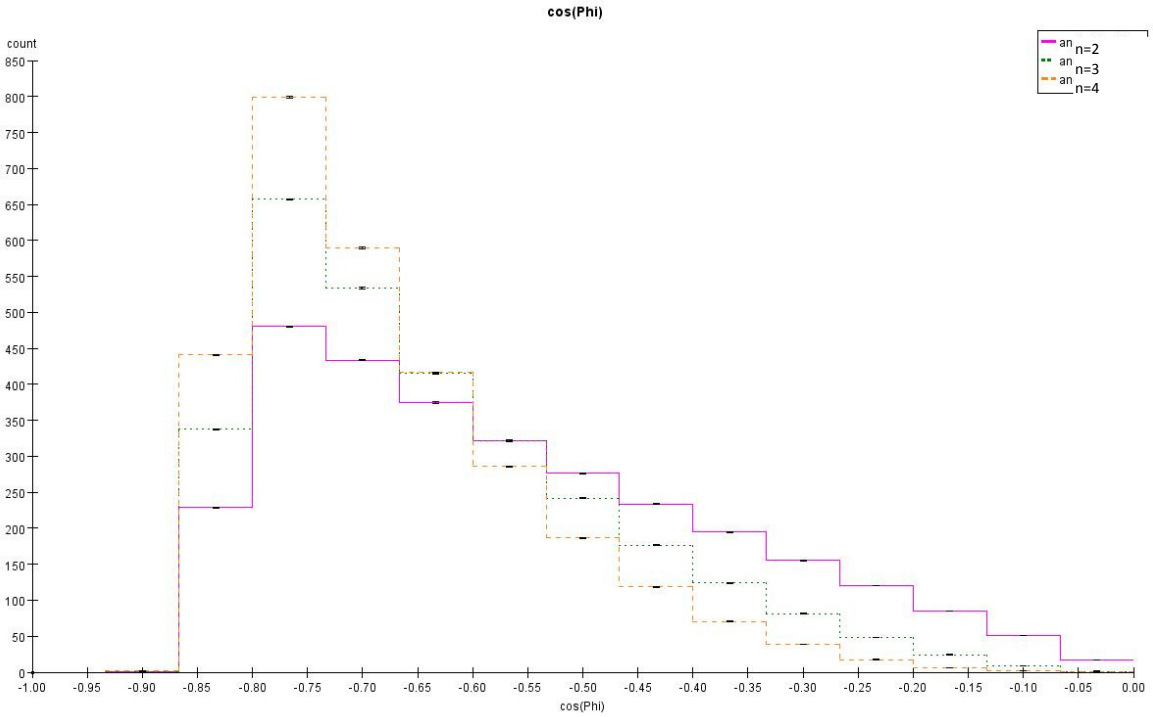

Figure 18. This is the plot of the monte carlo output for the measured distribution in the wall. The distribution is plotted for three values of n and are all normalized to the same total number of counts.

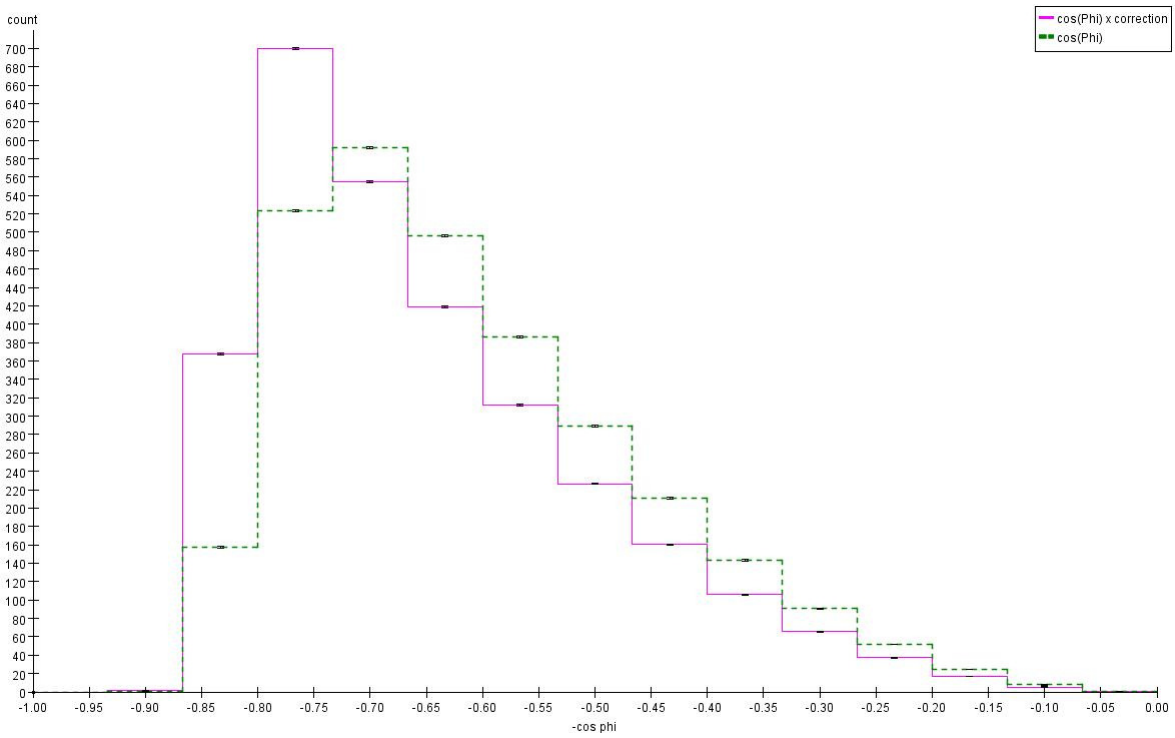

Figure 19. This histogram shows the difference in the real $\cos^n \phi$ distribution and the distribution detected in the wall data. The difference is caused by the lack of x data in the wall.

4.8 Zenith angle data

The zenith angle measurements are split into two sections, that from the ceiling and that from the wall. It is not possible to directly combine the two data sets because the wall data is distorted as seen in figure 19 from the Monte Carlo. It is possible to study the full range by using data individually from both sections. The ceiling is further split into a north-south section of data and an east-west section of data. This is done because of the differences of flux noticed in the azimuthal distribution. The sections of the detector used in each measurement are shown in figure 20.

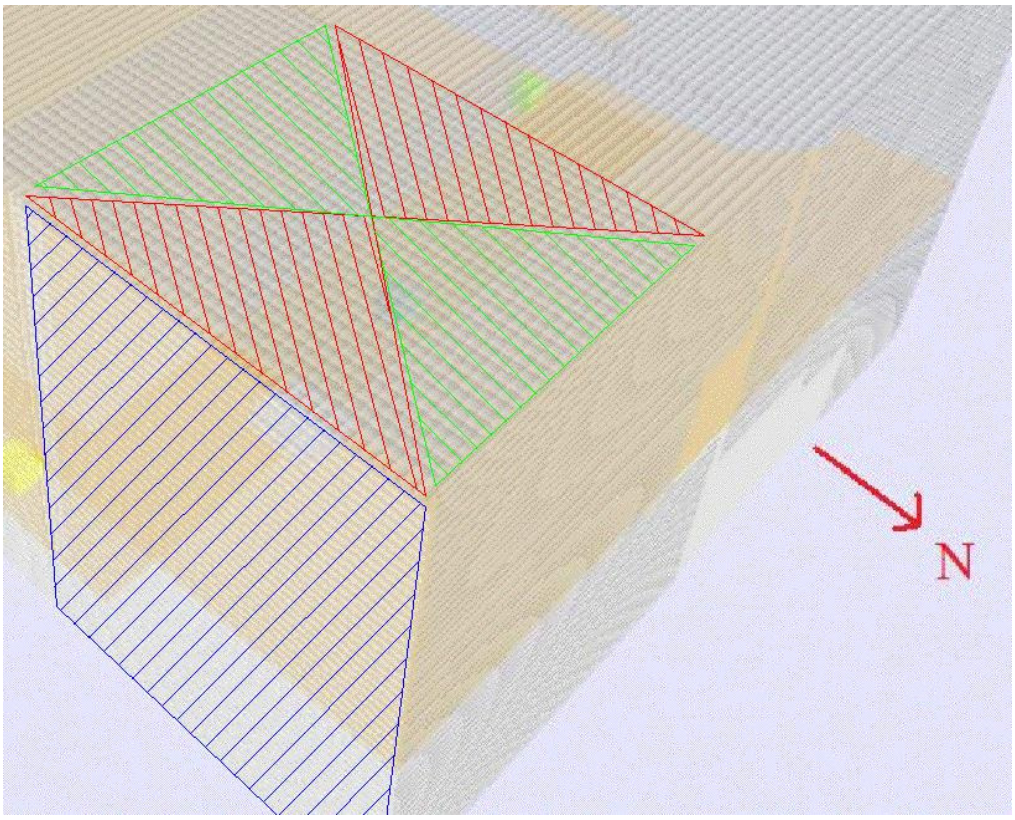

Figure 20. This picture gives a general breakdown of which regions of the detector are used for each measurement. The blue hatched section is the wall data, the green hatched region the north-south data and the red hatched region the east-west data. All these data sets of course include the test stack.

The first cut of data is the north-south data from the ceiling is shown in figure 21 along with $\cos^n \phi$ fits for comparison. This data comes from the green hatched region in figure 20.

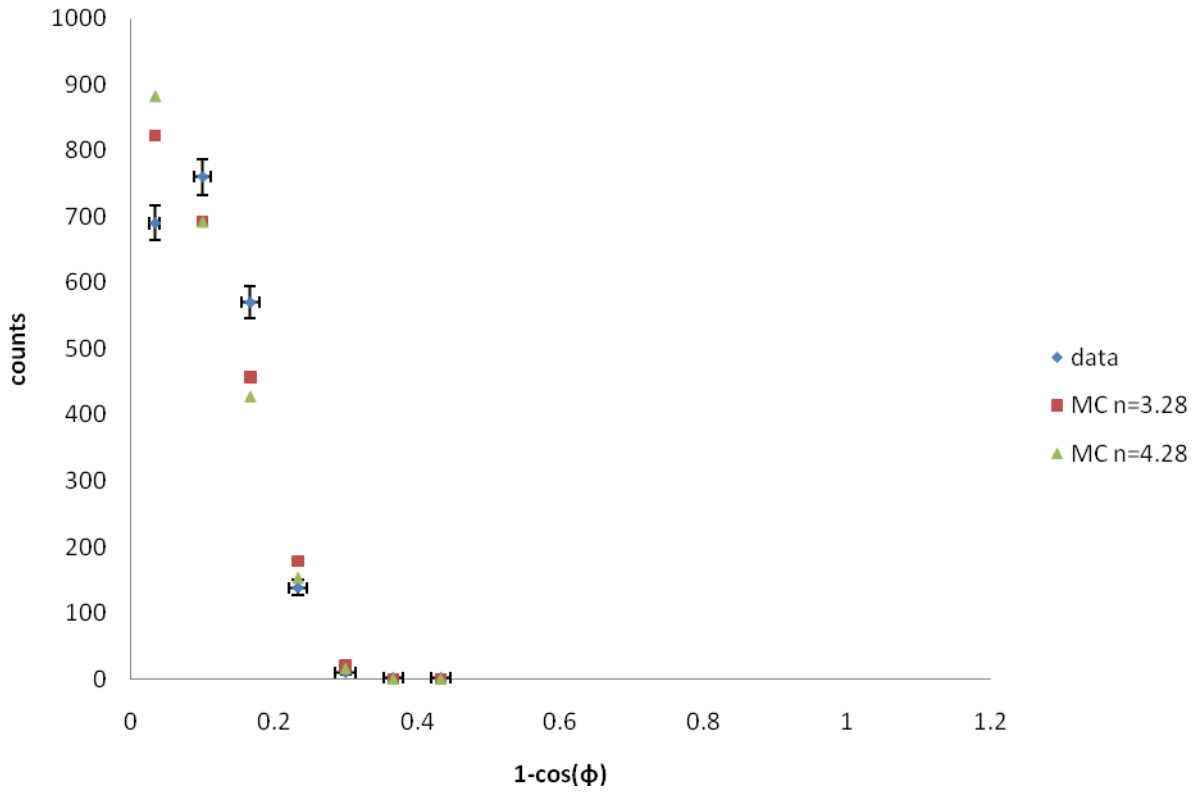

Figure 21. This figure shows the north-south zenith data. Two distributions from the Monte Carlo are shown in the plot as well.

The second set of data is the east-west data shown in figure 22 along with $\cos^n \phi$ fits for comparison. These data come from the red hatched region in figure 20.

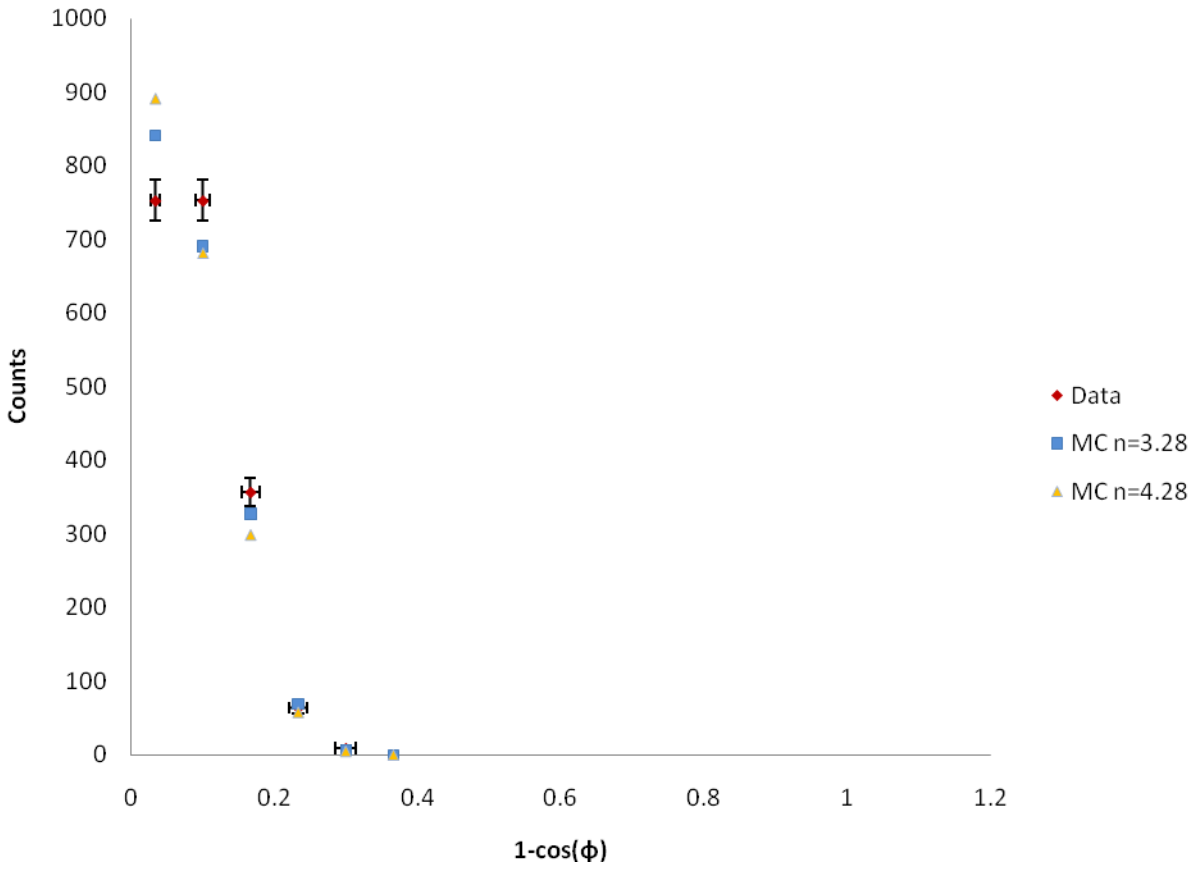

Figure 22. This figure shows the east-west zenith data. Two distributions from the Monte Carlo are shown in the plot as well.

The zenith data from the ceiling does not show a reasonable fit to the expectation shown in equation (6). The distributions are also too limited to attempt to fit with only five and seven data points. Any fit would have little meaning. We can see interesting features in the distributions though. The north-south and east-west data both show a deficiency in the vertical flux of muons. This deficiency in vertical ($\phi < 25°$) flux seems against the intuition because of the excavation above the lab has reduced its effective density, but the effects of the ridge and the higher density of the rock above the laboratory cause a greater effect. We can also see the differences in the fluxes between the two orientations; the two plots of zenith angle are combined in figure 23. The total number of events counted in the north-south direction is 2172 counts while in the east-west direction it is 1981 counts and the flux dies off more slowly north-south direction. This effect should only become stronger if we could look deeper in zenith angle because the effects of the ridge and east-west taconite deposits would become more pronounced.

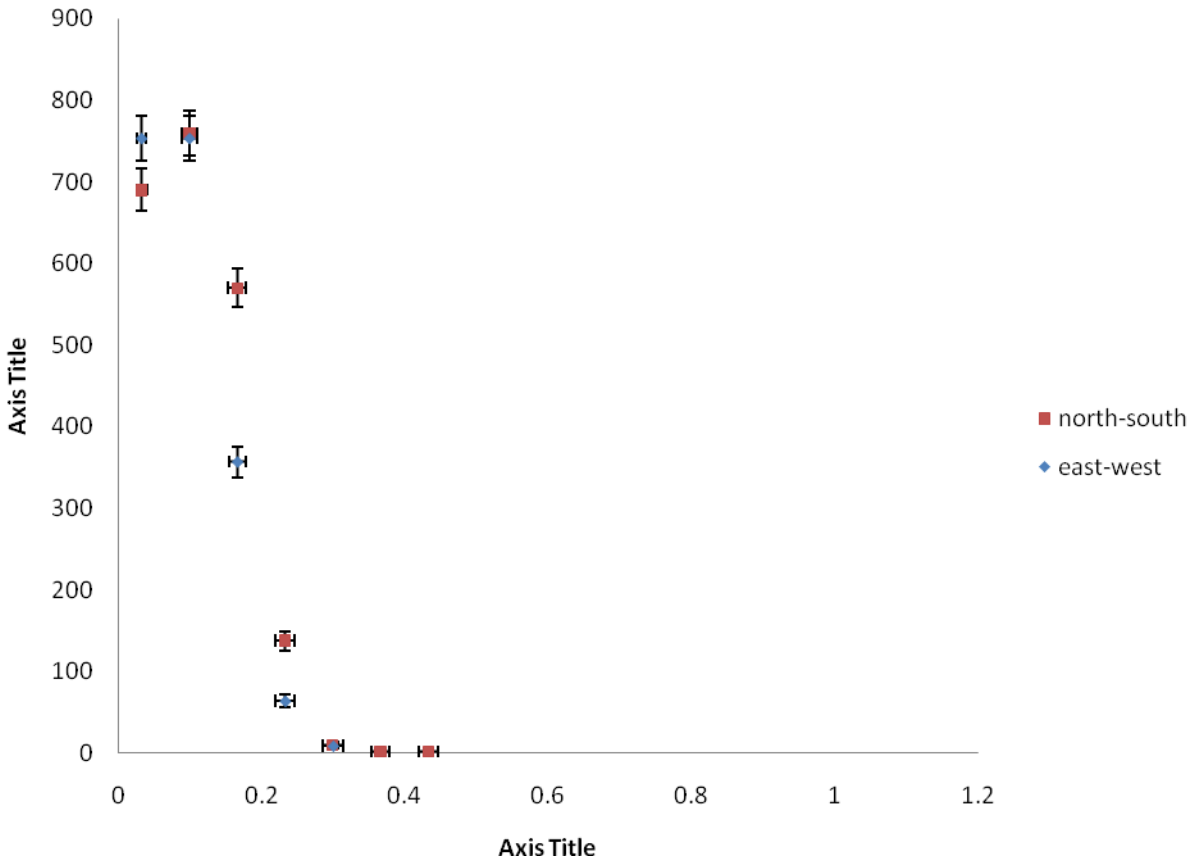

Figure 23. This plot compares the east-west and the north-south data.

The final set of data is the data coming from the wall. This data set gives us a wider range of zenith angle measurements, but it is distorted because of the lack of knowledge in the x direction as shown in figure 19. The Monte Carlo was used to predict the distribution which would be measured in the wall/test stack data as described above. The zenith data from the wall along with two Monte Carlo predictions are shown in figure 24. These data come from the blue hatched region of figure 20.

The first $\cos^n \phi$ fit is the n = 3.28 as predicted by Nelson, but we can see that this is not a good parameterization of this distribution. To get a better fit to the function, a least squares fit was used. This fit was accomplished by creating the expected distribution with the Monte Carlo for specific values of n and then calculating the χ^2 for the distribution. The fit excludes $1 - \cos \phi > 0.80$. This is due to the long tail on the distribution that is visible. It has been suggested that this tail is caused by neutrinos from the NuMi beam [8]. The χ^2 versus n plot is shown in figure 25. To reduce the statistical fluctuation in the Monte Carlo each data point is calculated with 100,000,000 muons generated. Read from figure 25, we find $n = 4.28 \pm 0.08$ but we find $\chi^2 = 20.16$. This corresponds to $\chi_r^2 = 2.52$. The fit to equation (6) is not good, but the function does capture the correct general features. Clearly we will require a much

more complicated parameterization. Furthermore, we already know that there are variations in the fluxes with azimuthal angle and the difference in shape of zenith distribution, so there will be no simply analytic expression to represent the entire distribution.

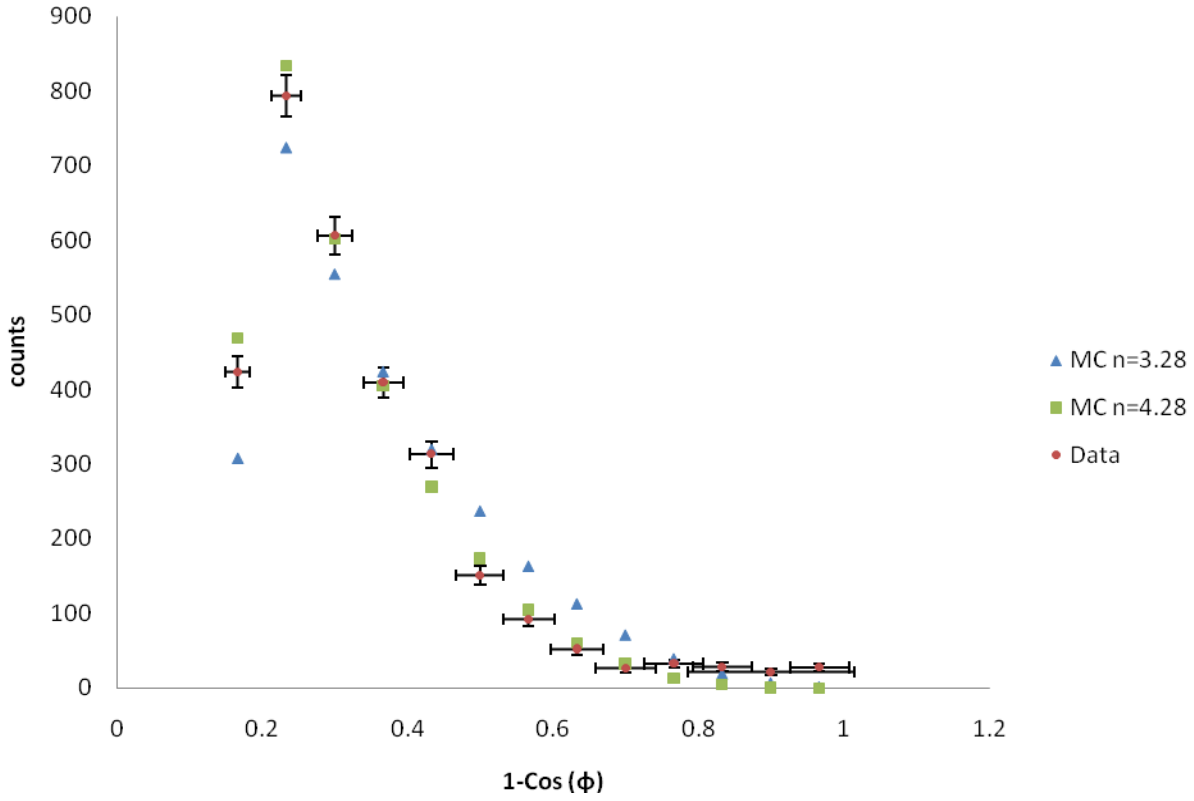

Figure 24. This plot shows the zenith distribution measured with the wall in the east west direction. There are two Monte Carlo predicted distributions. The n = 4.28 ± 0.8 distribution is the best fit to the data.

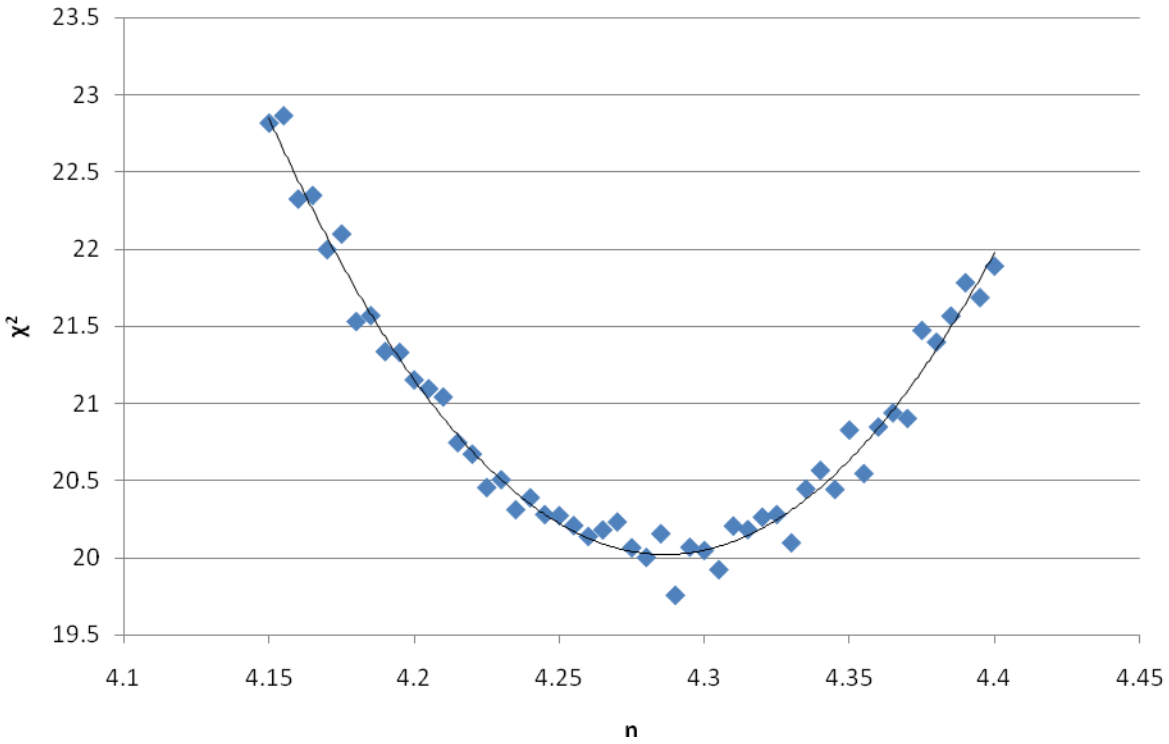

Figure 25. This is a plot of χ^2 vs. n for the fit of the Monte Carlo predicted distribution to the measured distribution in east-west zenith angle data from the wall.

4.9 Angle conclusion

The angular distributions measured by the vetoshield do make reasonable qualitative agreement with the expectations from both the basic Monte Carlo and geographic considerations. This gives us confidence in the proper operation of the shield and the DAQ. The azimuthal distribution of the Soudan Lab favors the north-south direction over the east-west direction, in line with the alignment of geologic barriers. We also see that the zenith distribution in the east-west direction corresponds to a deeper effective depth than the north-south direction. This is further enforced by the wide angle data from the wall in the east-west direction where the best possible approximation to the distribution follows with $n = 4.28 \pm 0.08$ instead of the $n = 3.28$ predicted for more vertical muon flux by Nelson. It should be remembered that the $n = 4.28$ measurement only applies to the east-west direction for zenith angles greater than about 35° or so. In general the entire angular distribution cannot be fit to simple analytic function.

With the angular measurements, we can benchmark the muon distributions used in the full Monte Carlo simulations for experiments at Soudan. Different Monte Carlos use different input distributions for their angular maps and it would be useful to have a general angular distribution for all the Soudan Monte Carlos. Although this data is insufficient on its own to construct such an angular map, it does provide the ability to check and adjust existing distributions. In order to improve these measurements the setup will continue to take data, now with the second generation DAQ. The north wall repairs will also be completed this coming summer to allow data from the north wall to be collected and have a more complete picture in the north-south direction. We would expect that the north-south wall distribution would correspond to a more shallow distribution. Another general interest measurement that can be done is to study the large angle tail by only looking at data during NuMi beam spills to determine if these events are caused by beam muons.

Chapter 5

High Multiplicity Measurements

5.1 High multiplicity introduction

Experiments in the deep underground setting naturally have lower background than their above ground counterparts, but going underground adds new problems. Hadronic showers produced in the rock above the cavern can have high energy neutrons associated with them along with the charged particle showers. While the charged particles are easily blocked or vetoed, the fast neutrons can make it through low Z shielding and interact with detectors in undesirable ways. This type of background is especially dangerous to WIMP searches where a neutron scatter inside the detector mass could be mistaken for a WIMP.

The CDMS collaboration along with other low background underground experiments is attempting to quantify these fast neutrons by means of Monte Carlo simulations of showers which cause such neutrons. The primary codes being used to do these simulations is the GEANT4 code and the FLUKA code, but there are very large discrepancies in the predictions between these two codes as large as a factor of 2 or 3. These differences require further data to benchmark the results. Along with the angular measurements we have also been studying the high multiplicity showers in the vetoshield to better understand them.

5.2 High multiplicity data

The data for the high multiplicity study taken so far comes from the same data run as the angle data, so the shield configuration and trigger setup are the same. With the trigger on the test stack we

preferentially get showers that originate above the test stack, so we have limited this early analysis to the showers that are confined to the ceiling and will not seriously look at the data from the wall. In future data runs where we are using the new DAQ and are able to better control the triggers and the data influx into the computer we can trigger on more panels at the same time.

The first step in understanding these shower backgrounds is to understand how we detect these showers. The vetoshield gives us no energy information about events so we must rely entirely on the positional information to learn about the events. This starts by actually looking at the events in the 3D viewer and beginning to understand the different forms the high multiplicity events take in the shield. From this phenomenological view of the system we see that there are two general groupings of high multiplicity events in the shield: clustered events and diffuse events.

The clustered events, such as those shown in figure 26, consist of a tight grouping of events that shows up in both layers of the ceiling or as a tight cluster in the wall. It is not uncommon like in the case in figure 26 to have a cluster in the ceiling as well as another corresponding cluster in the wall. These events correspond to what we would expect to see from a hadronic shower originating in the rock just above the shield and spraying the cavern with charged particles. Thus we associate these events with real showers originated above the cavern.

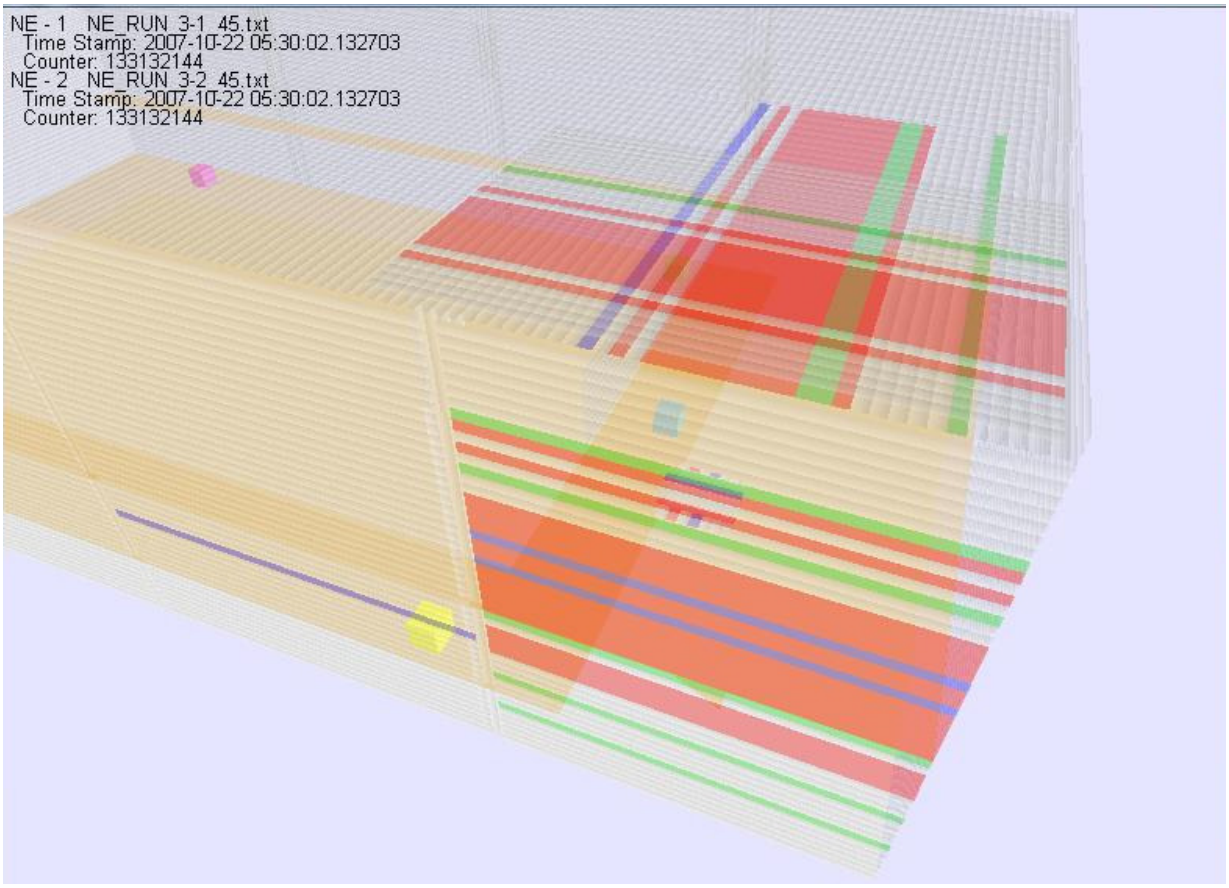

Figure 26. This is a "clustered" event in the veto shield. We can see where the primary cone of the shower in the ceiling and more spray brushing the wall.

Diffuse events, such as the event shown in figure 27, are events which have no definite center. They are often events where the majority of a panel, or in fact all panels, will go high at the same time. Events such as this are usually caused by noise. We have confirmed for instance that welding near the shield can cause huge noise spikes such as the event shown in figure 27. Although most of these events are attributable to noise in the system, we cannot say they all are noise. Any events which happen farther in the rock will filter out all events but the muons and cause a number of clear spaced events.

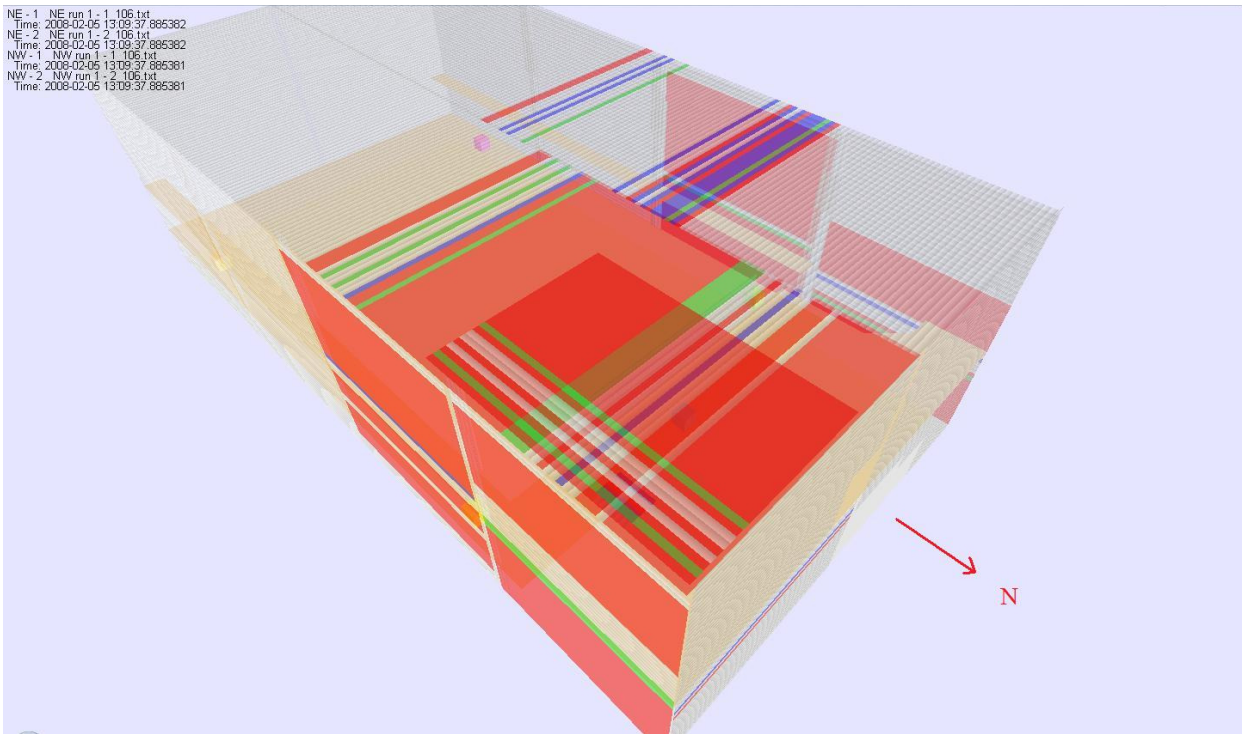

Figure 27. This is a "diffuse event." This event is noise induced from welding around the shield, but not all diffuse events are this large nor are all linked to noise sources.

The biggest challenge we currently face is to find a cut which will separate the noise events from the real showers. With the extremely limited amount of data available from the vetoshield we have little to work with. The best criterion for this cut is a requirement similar to that used in the angular distribution measurements. This is to require that there be at least one hit in each layer of the ceiling and at least one hit in two of the three layers of the test stack. This gives us good confidence that there was a muon associated with the event. Unlike the angle events there is no limit on the number of hits.

The multiplicity of the event is the only other quantity we have to work with in cutting this data. Histograms of the multiplicities of the two panels above the test stack are shown in figure 28. This figure shows the multiplicity before and after cutting the data by requiring that there be a muon in the event. The two purple histograms are uncut and contain every data point taken. The green plots are made with the cut described above. Because of the high rate of noise in the tubes, most of the triggers in the test stack yield no hits in the ceiling. The requirement that there be a muon removes this large background from our data as can be seen in the lower plots. In the upper uncut data we also see a very large tail, especially in panel 7 (which has more tubes than panel 43). In this region we see that the multiplicity does not taper off anymore but continues to the end of the plot. This tail is largely filled

with noise events which are not related to physical events but to electrical noise in the tubes or DAQ. The cut also filters out most all of this noisy tail. Finally, we note that although the total amount of data was reduced by a factor of 10^4 or so, the high multiplicity events are only reduced by a factor 10 to 10^2, but much of the lost high multiplicity data lost would be noise. This is because, while triggering of the test stack, any trigger event in the ceiling without a muon in the test stack is simply a random sample.

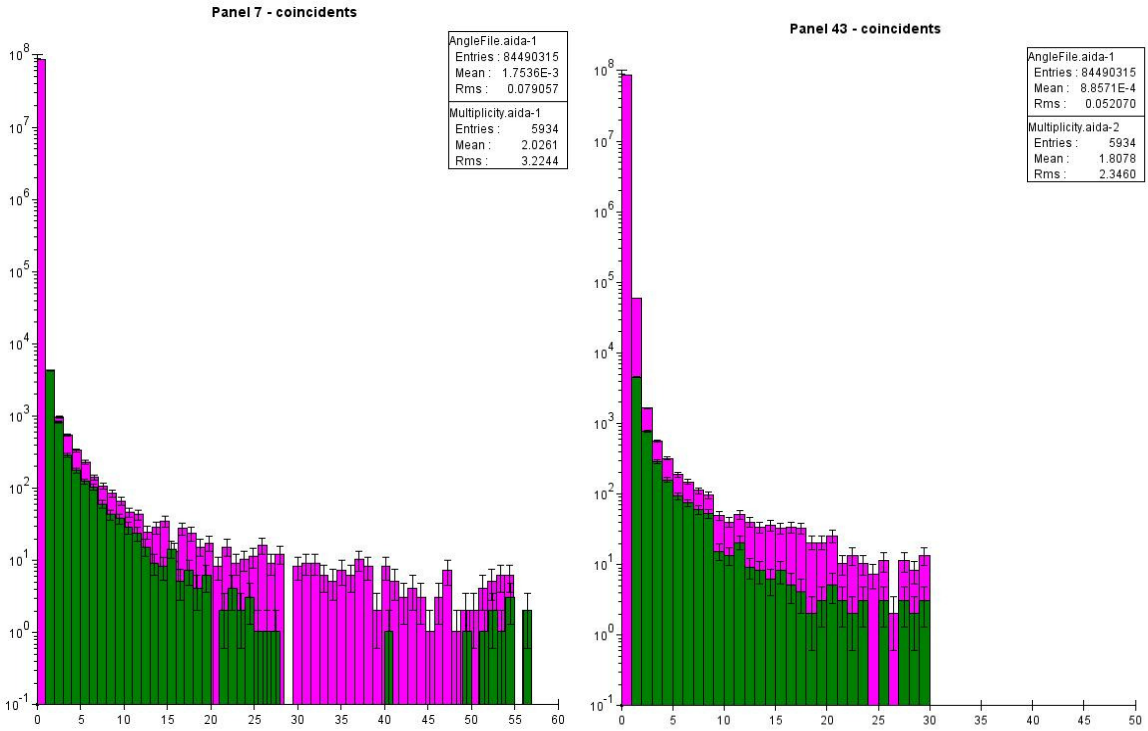

Figure 28. These plots show the multiplicity histograms of coincident in the two layers of the ceiling above the test stack. The purple plots include the uncut multiplicity data. The green plots are cut to include only events with muons in the test stack. Panel 7 has 54 tubes while Panel 43 only has 29.

These events can be compared to a monte carlo simulation of these events in the vetoshield which would be capable of telling us what we are actually seeing in these events. With the vetoshield alone we have no way to id particles. Even a muon cannot be identified in such a shower because individual events are drowned out in the mass of hits. In order to study these showers and the neutrons associated with them we will need something more, luckily more is on the way.

5.3 Neutron Multiplicity Meter

The Neutron Multiplicity Meter is a gadolinium-loaded liquid-scintillator neutron detector which is being built by UC Santa Barbra and Case Western Reserve. The detector itself will detect low energy neutrons which will be produced by high energy neutrons interacting with a stack of lead. The high energy neutrons create showers in the lead which then produces more neutrons. These neutrons etherealize over about 40 µs and are captured in the gadolinium-loaded liquid-scintillator. The scintillator is then readout with a phototube on the each end of the device [9]. A schematic of the Neutron Multiplicity Meter is shown in figure 29.

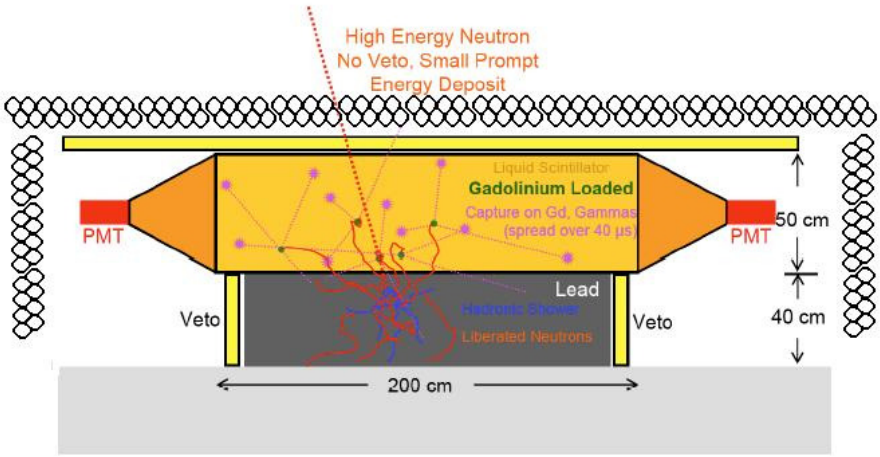

Figure 29. This is a schematic of the Neutron Multiplicity Meter and the shield around it. The detector consists of the large box filled with gadolinium-loaded liquid-scintillator to detect the thermal neutron and the lead base to "catch" the high energy neutrons. There is also the electromagnetic veto provided with the shield [10].

This detector, which will contain four 50 × 50 × 200 cm detector tanks, will be placed in the Soudan LBCF where it will measure high energy neutron flux. In the LBCF the Neutron Multiplicity Meter will benefit from the charged particle detection available from the vetoshield. If the funding is approved the Neutron Multiplicity Meter will be surrounded with a set of extra short veto tubes which will be

readout with the rest of the shield DAQ. This will provide a setup similar to the test stack setup used to measure the angular distribution, but it will also have the ability to measure neutrons present in the showers. The shield also gives the advantage us having a large lever arm to see where shower components came from that cannot be achieved with small vetoes around the detector itself. The shield also removes any confusion in the signal caused by muons interacting with the detector and lead [11]. This setup will allow us to look at electromagnetic components of the showers and the neutron flux at the same time and compare the way they are related. It is hoped that we will be able to relate the electromagnetic presence to the presence of neutrons and so help to shield the CDMS experiment and others more effectively. The first prototype detector for the Neutron Multiplicity Meter will be installed in late summer 2008.

Chapter 6

Conclusion

The vetoshield has been refurbished and the tubes are in working order. We have also designed and tested the new DAQ system for the shield which is designed to operate in the multi-user oriented environment. This DAQ is flexible and cost effective. It should serve the LBCF will in its future operation.

We have successfully measured the angular distribution of muons in the Soudan Laboratory using the refurbished muon vetoshield. This distribution conforms to the expectations beforehand that the flux should be higher in the north and south directions and that the east-west distribution at large angles corresponds to a much deeper distribution than would be predicted by looking at the vertical flux. Finally, we proved that the shield is capable of detecting high multiplicity showers and began to characterize these showers in preparation for the Neutron Multiplicity Meter.

With these angular distributions along with the high multiplicity data prove that the shield is in working order and still capable of carrying out physics. The angular distribution, existing and future, along with the information from the Neutron Multiplicity Meter will hopefully finally provide a proper benchmark for the neutron background simulations and allow this problem to be put to rest.

Bibliography

[1] P. Cushman, “DUSEL R&D – Benchmarking Hadronic Showers Underground: Correlating cosmogenic neutron production with high multiplicity showers,” Research proposal, 2007 (unpublished).

[2] R. Nelson, “The Veto System Pulser and Studies of Deep Underground Muons for the CDMS-II Experiment,” B.S. Thesis US Santa Barbara, 2003.

[3] P. Cushman, “Comparison of the Input Moun Distributions used for CDMS Neutron Simulations,” 2006 (unpublished).

[4] P. Cushman, “Comparison of the Input Moun Distributions.”

[5] K. Ruddick, “Underground Particle Fluxes in the Soudan Mine,” NuMi-L-210, September 1996 (unpublished).

[6] USGS Topographical Map, 1986.

[7] R. Nelson.

[8] P. Litchfield, Private Communication.

[9] P. Cushman, “DUSEL R&D.”

[10] P. Cushman, “DUSEL R&D.”

[11] P. Cushman, “DUSEL R&D.”